Progress in Oceanography xxx (2017) xxx–xxx

Contents lists available at ScienceDirect

Progress in Oceanography

journal homepage: www.elsevier.com/locate/pocean

Determining Atlantic Ocean province contrasts and variations

Tim Smyth [a,*], Graham Quartly [a], Thomas Jackson [a], Glen Tarran [a], Malcolm Woodward [a], Carolyn Harris [a], Chris Gallienne [a], Rob Thomas [b], Ruth Airs [a], Denise Cummings [a], Robert Brewin [a], Vassilis Kitidis [a], John Stephens [a], Mike Zubkov [c], Andrew Rees [a]

[a] Plymouth Marine Laboratory, Prospect Place, Plymouth, Devon PL1 3DH, UK
[b] British Oceanographic Data Centre, Joseph Proudman Building, 6 Brownlow Street, Liverpool L3 5DA, UK
[c] National Oceanography Centre, Waterfront Campus, European Way, Southampton, Hampshire SO14 3ZH, UK

ARTICLE INFO

Article history:
Available online xxxx

ABSTRACT

The Atlantic Meridional Transect (AMT) series of twenty-five cruises over the past twenty years has produced a rich depth-resolved biogeochemical *in situ* data resource consisting of a wealth of core variables. These multiple core datasets, key to the operation of AMT, such as temperature, salinity, oxygen and inorganic nutrients, are often only used as ancillary measurements for contextualising hypothesis-driven process studies. In this paper these core *in situ* variables, alongside data drawn from satellite Earth Observation (EO) and modelling, have been analysed to determine characteristic oceanic province variations encountered over the last twenty years on the AMT through the Atlantic Ocean. The EO and modelling analysis shows the variations of key environmental variables in each province, such as surface currents, the net heat flux and subsequent large scale biological responses, such as primary production. The *in situ* core dataset analysis allows the variation in features such as the tropical oxygen minimum zone to be quantified as well as showing clear contrasts between the provinces in nutrient stoichiometry. Such observations and relationships can be used within basin scale biogeochemical models to set realistic variation ranges.

1. Introduction

The importance of the Atlantic Ocean as a climate regulator (Bryden et al., 2005), food source region (Fromentin and Powers, 2005), and its historical significance for trade routes, cultural diffusion and military conflicts (Winchester, 2011), is difficult to overstate. This ocean basin supports an extreme diversity of lifeforms from the smallest microbes to the largest mammals on the planet. It receives freshwater from several of the world's largest catchments (including the Amazon and Congo), contains the hydrographically and geologically important mid-Atlantic Ridge, and boasts several Islands (Ascension, St. Helena, Falklands, S. Georgia) and Island Chains (Azores, Canaries, Cape Verde). It is against this backdrop that the Atlantic Meridional Transect (AMT) occurs with the express aim of observing basin scale variability and change to inform on societally important concerns such as climate change, biodiversity, productivity and ecosystem functionality. At this time in its history, the strengths of the AMT are: the longevity of the programme and; its uniqueness in sampling across a wide range of biomes, from highly productive mid-latitude provinces to the oligotrophic gyres in the tropical and sub-tropical regions. However, observing basin scale variability and change using the past twenty years of the Atlantic Meridional Transect data is a particularly challenging task for three reasons.

Firstly, changes to the expedition route: this is as a result of an evolution of priority research questions over time and the logistical constraints offered by research vessel management. The early series (AMT01–11; between 1995 and 2000) had an emphasis on ocean colour satellite validation before and after the launch of the Sea-viewing Wide-Field-of-view Sensor (SeaWiFS) in September 1997: expeditions were six monthly and were both south-to-north (boreal spring) and north-to-south (boreal autumn). The middle series (AMT12–17; between 2003 and 2005) were multi-directional, but focussed on biogeochemical processes such that some cruises passed through the oligotrophic gyres and others traversed regions of intense productivity such as the Benguela and Mauritanian upwellings. The latest series (AMT18; from 2008 onwards) have all been north-to-south (boreal autumn) and research questions related to the Atlantic oligotrophic gyres have dominated. This first challenge may be described as longitudinal aliasing.

Secondly: seasonal aliasing. The south-to-north expeditions take place in the austral autumn (boreal spring), whereas the

* Corresponding author.
E-mail address: tjsm@pml.ac.uk (T. Smyth).

http://dx.doi.org/10.1016/j.pocean.2016.12.004
0079-6611/

north-to-south occur in the boreal autumn (austral spring). The exact timings and lengths of the cruises have also altered, constrained by logistical and financial considerations. The shortest duration expeditions were approximately of order 30 days, whereas the longest closer to 50 days. The start and end dates also varied by more than a month in some instances. Although this may seem insignificant, the equinoxes mark the periods of greatest biotic and abiotic change in both hemispheres, thereby increasing the potential for seasonal aliasing.

Thirdly: variable inconsistency. Electronically-derived variables measured on a typical oceanographic profiler (often itself referred to as "the CTD") such as temperature and conductivity (oxygen and fluorescence) are fairly straightforward to subsample at well-ordered and evenly spaced depths. Other variables (nutrients, pigments, flow cytometry) require discrete samples to be taken from Niskin bottles triggered at different depths through the water column. As the AMT programme has been dominated by biogeochemistry from the outset these sampling depths tend to change depending on different light levels (e.g. 97%, 55%, 33%, 14%, 7%, 3%, 1% and 0.1% of surface irradiance) through the water column rather than fixed geometric depths. For example, the euphotic depth (1% light depth) in the oligotrophic gyres may exceed 150 m, whereas in the productive shelf seas and upwelling regions this depth may be less than 50 m. Again, as the programme has evolved over time, the number and type of variables has changed accordingly. Therefore, there are only a few select core variables which have been measured consistently on a large enough subset of the 25 cruises to perform an analysis. From the *in situ* dataset we have selected temperature, salinity, oxygen, fluorescence, nutrients, flow cytometry, pigments and Optical Plankton Counter data, which are relevant to GOOS-IOCCP Essential Ocean Variables (EOVs) and also cover many of the UK Integrated Marine Observing Network initiative (UKIMON) recognised core variables.

Each of these three challenges: longitudinal aliasing, seasonal aliasing and variable consistency, could possibly lead to the conclusion that, despite twenty years of the Atlantic Meridional Transect, the dataset is too fragmented and sparsely sampled to be of any use to observe basin scale variability. In essence all we are achieving is drawing a thin observational curtain down multiple routes, once, possibly twice a year at the time of most dynamic seasonal change. However, that would underestimate the richness of the data set: the longevity of the time-series itself, together with its multiple visits to the same bio-geographical regions, has allowed a statistically significant amount of multi-variable data to be collected to enable broad generalisations to be constructed.

The *in situ* AMT dataset yields unparalleled depth-resolved biogeochemical information on the basin-scale pelagic Atlantic Ocean but it is time and space-scale limited. Therefore to achieve our aim of quantifying Atlantic Ocean basin scale variations and contrasting the different provinces, we have used additional datasets of satellite remote sensing (Earth Observation – EO) and modelling to complement the *in situ* data.

EO data provide synoptic scale coverage on time-scales of days to years at sub-mesoscale (1–10 km) spatial resolution. However, both active (e.g. radar) and passive (e.g. ocean colour) forms of remote sensing are depth-limited to a thin skin of the surface ocean because of the inability of electromagnetic radiation to penetrate more than a few tens of metres at optical frequencies and a few millimetres in the infra-red and radio-frequencies. Ocean models can provide time, horizontal and vertical dimensional data on scales of minutes to centuries, metres to thousands of kilometres. However, they are limited by the extent of our knowledge, our observational capacity and our ability to accurately capture sometimes poorly understood processes and making them numerically tractable (i.e. our ability to programme a computer, and computer processing power).

In order to usefully quantify Atlantic Ocean variations, using these three broad sources of data, we use as a framework the concept of oceanic provinces which is most often associated with the work of Longhurst (1998). Although many papers have recently appeared in the literature arguably improving on his work which in essence allow a form of deterministic elasticity at the boundaries between ocean provinces (Hardman-Mountford et al., 2008; Reygondeau et al., 2013), in this paper we will retain the concept of rigid boundaries as implementing these different schemes will only serve to add unnecessary complexity to our data analyses. These so-called Longhurst provinces are shown in Fig. 1: for the purposes of this paper we will be concentrating on the provinces which contain most data. These are, from north to south: (i) North Atlantic Drift Region (NADR); (ii) North Atlantic Sub-tropical Gyre, East (NASE); (iii) North Atlantic Tropical Gyre (NATR); (iv) Western Tropical Atlantic (WTRA); (v) South Atlantic Gyre (SATL) and; (vi) South Sub-tropical Convergence (SSTC).

At this point it is useful to make a distinction between the terms variability and variations. Variability, especially within the context of a long-term programme such as AMT, carries connotations of climate or ecosystem change. In this paper we are not attempting to address long-term variability associated with these large scale drivers, as these are certainly stymied by longitudinal and seasonal aliasing. Rather we are investigating the spatial (i.e. across entire provinces) and temporal (i.e. over multiple annual cycles) variations in key observables: an inevitable result of the AMT expedition route covering such large gradients. This then allows us to contrast the different Atlantic provinces.

2. Methods

An adequate analysis of province scale variations requires the use of suitable metrics to describe variables which have very different characteristics. *In situ* observations are strongly tied to a single geographical location and time; EO and model observations allow multiple, spatially distributed, observations at a given time. EO and model observations are repeated right across a given province at frequent time intervals (daily, weekly, monthly) and are easily aggregated in time and space onto a consistent grid; *in situ* observations are rarely repeated in the same location (longitudinal aliasing), and are not widely distributed in time and space across any given province (longitudinal and seasonal aliasing).

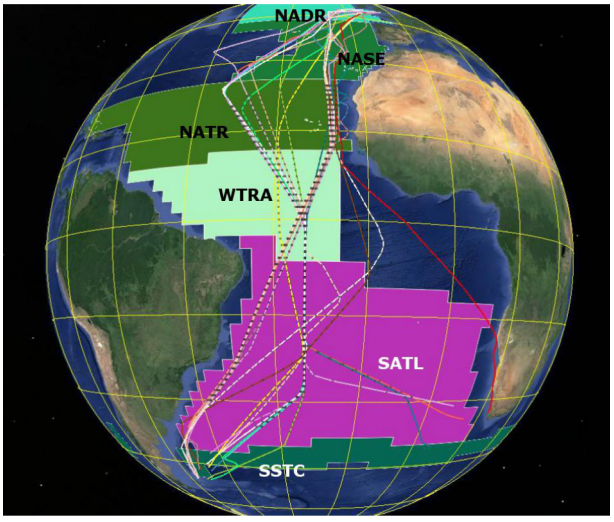

Fig. 1. Map of the Longhurst provinces under investigation with the various AMT cruise tracks superimposed. Background image courtesy of Google Earth.

Please cite this article in press as: Smyth, T., et al. Determining Atlantic Ocean province contrasts and variations. Prog. Oceanogr. (2017), http://dx.doi.org/10.1016/j.pocean.2016.12.004

In this paper we widely use the standard deviation to describe variation. For the EO and model imagery this can be represented on a pixel-by-pixel basis (e.g. Fig. 3) and then aggregated up to produce a province wide "mean" standard deviation (e.g. Fig. 4). For the *in situ* data, the vertical profile mean and standard deviation are calculated (temperature and salinity, oxygen, chlorophyll fluorescence) as a metric of variation. These data rich *in situ* sources are typically available at 1 m depth resolution through the water column whereas parameters such as inorganic nutrients, pigments and flow cytometry are reliant upon samples taken at discrete depths (generally 10–20 per vertical profile). This further complicates the definition of variation. Therefore

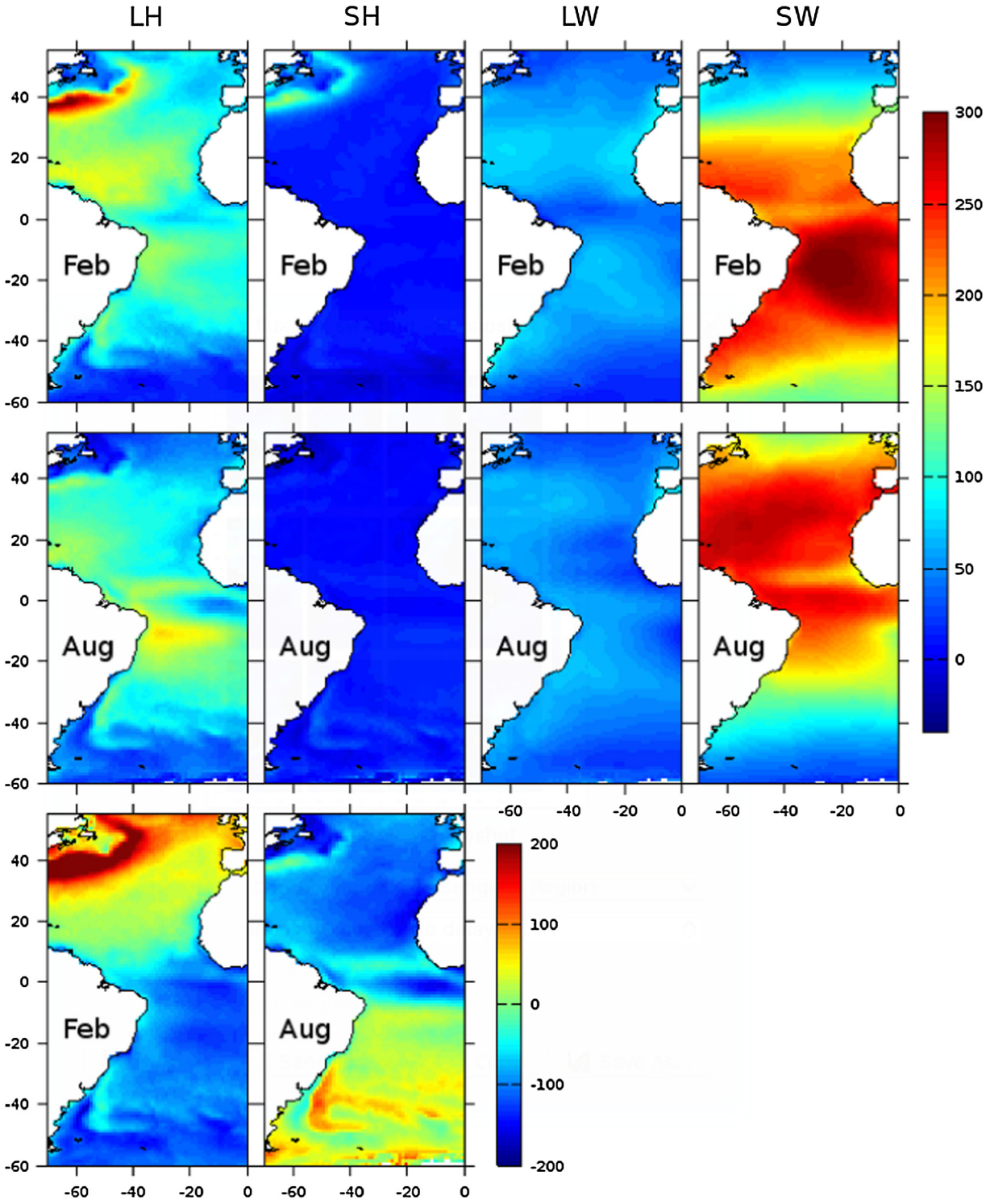

Fig. 2. Calculated monthly mean surface heat flux (units W m^{-2}) components of Latent (LH), Sensible (SH), Longwave (LW) and Shortwave (SW) for February and August over the period 1998–2007. Bottom two panels are the Net Heat (NH) flux. LH, SH, LW and NH use the convention of positive out of the water column, SW is positive into the water column. (See web version of this article for colour.)

Please cite this article in press as: Smyth, T., et al. Determining Atlantic Ocean province contrasts and variations. Prog. Oceanogr. (2017), http://dx.doi.org/10.1016/j.pocean.2016.12.004

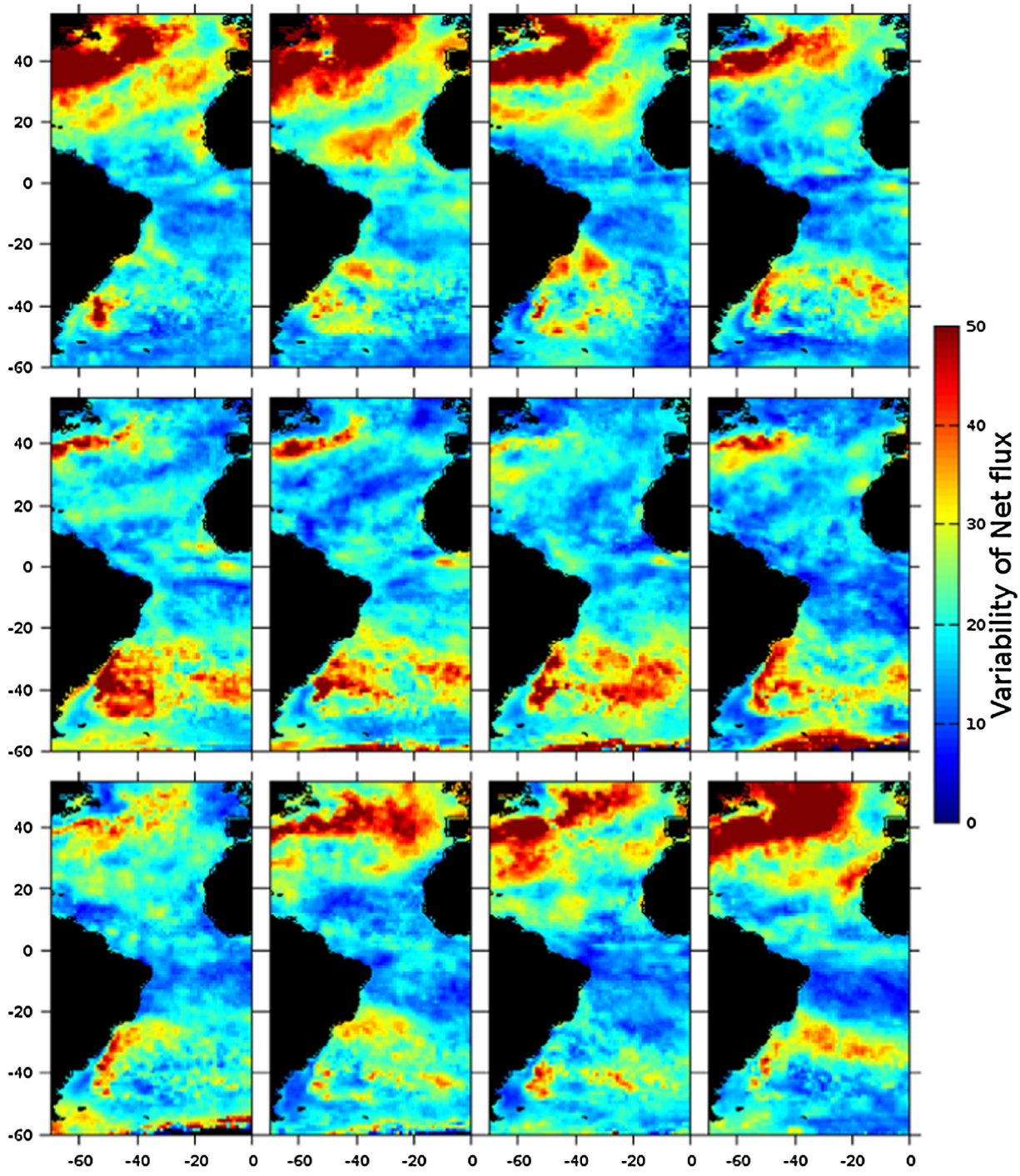

Fig. 3. Variation in the modelled Net Heat (NH) Flux (units W m^{-2}) calculated as the standard deviation from the monthly climatologies (1998–2007). Top row: January–April; middle row: May–August; bottom row: September–December. (See web version of this article for colour.)

for these parameters we have resorted to stoichiometric ratios (nutrients), pigment ratios, taxonomic ratios (flow cytometry) and size distribution (optical plankton counter) and rely upon regression statistics and visual presentation to describe province variation.

The different datasets have been grouped into large scale physical drivers (Net Heat Flux (modelling), Currents (EO)), large scale biological responses (Primary Production (EO)) and *in situ* measured responses (temperature and salinity, oxygen, chlorophyll fluorescence, inorganic nutrients, flow cytometry, pigments and Optical Plankton Counter).

3. Modelling

3.1. Net heat flux

Objectively analysed daily heat flux values (Latent, Sensible, Longwave and Shortwave components) (Yu et al., 2008) were obtained from the OAFlux project website (http://oaflux.whoi.edu/). The heat flux values are derived using the COARE bulk flux algorithm (Fairall et al., 2003) on a $1° \times 1°$ global ocean coverage grid with input values of windspeed (U), air temperature (T_a), sea-surface temperature (T_s) and humidity (q_a) obtained from

Please cite this article in press as: Smyth, T., et al. Determining Atlantic Ocean province contrasts and variations. Prog. Oceanogr. (2017), http://dx.doi.org/10.1016/j.pocean.2016.12.004

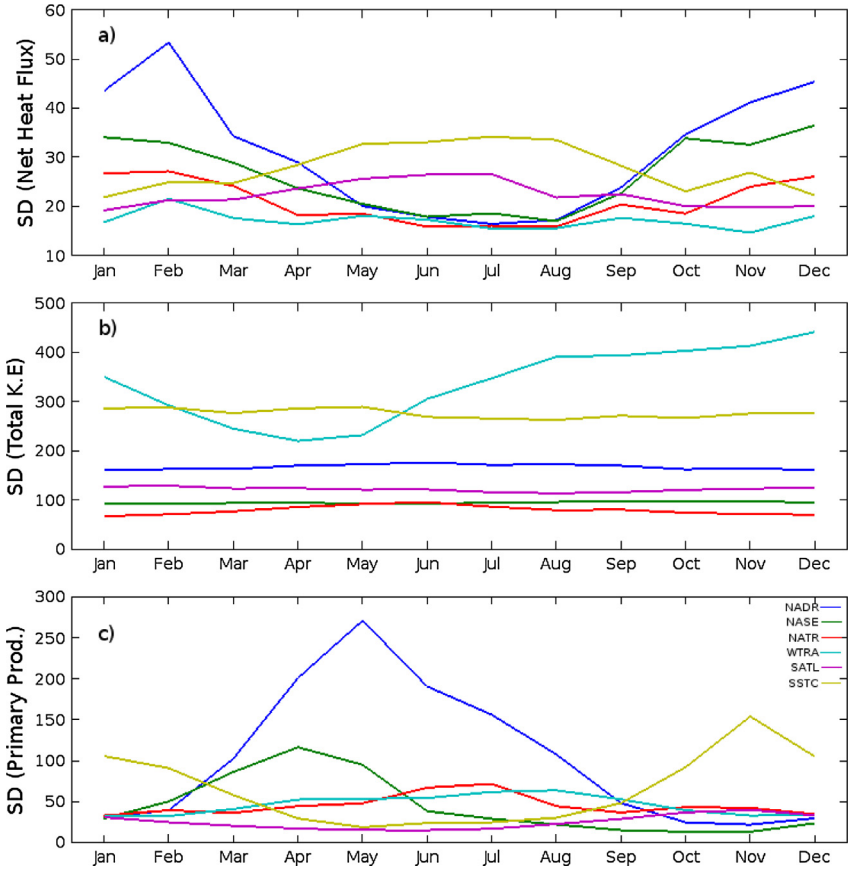

Fig. 4. Monthly variation (standard deviation) in monthly model and EO derived fields for six Longhurst provinces. (a) Net Heat Flux (W m^{-2}); (b) Total Kinetic Energy (cm^2 s^{-2}) and; (c) Primary Production (mg C m^{-2} d^{-1}). (See web version of this article for colour.)

surface meteorological fields derived from satellite remote sensing and reanalysis outputs produced from NCEP (National Center for Environmental Prediction) and ECMWF (European Centre for Medium Range Weather Forecasting) models. The OAFlux project applies an objective analysis approach to take into account data errors in the development of enhanced global flux fields. The objective analysis denotes the process of synthesising measurements/estimates from various sources. Such a process reduces error in each input data source and produces an estimate that has the minimum error variance. The OAFlux project uses the objective analysis to obtain optimal estimates of flux-related surface meteorology and then computes the global fluxes by using the state-of-the-art bulk flux parameterisations.

The daily values of latent heat (LH), sensible heat (SH), longwave radiation (LW) and shortwave radiation (SW) flux were then used to produce monthly mean climatologies for the period 1998–2007, with the intention of overlapping with the continuous operational period of the SeaWiFS mission. The net heat (NH) flux component was calculated from the four individual components.

In order to determine the typical variation, the standard deviation was calculated for each heat flux component (LH, SH, LW, SW) and the total net heat (NH) flux, for each climatological month on a pixel-by-pixel basis. The mean of the standard deviation was then calculated for each month on a province by province basis.

4. Earth Observation

4.1. Currents

Ocean currents provide one of the sources of mixing processes in the surface ocean. Within the whole realm covered by AMT there are a wide variety of current regimes from the large-scale gyral circulation in the North and South Atlantic basins, with broad coherent flows, to intense western boundary currents (WBC) such as the Gulf Stream and the Brazil Current. In addition to this mean flow there is considerable variation with meanders and eddy generation in the Gulf Stream (Leterme and Pingree, 2008), the interaction of two currents in the Brazil-Falklands Confluence (Garzoli and Garraffo, 1989) and the many energetic processes in the Equatorial region (Arnault and Kestenare, 2004). Satellite altimetry is a key technique for measuring the geostrophic currents, although the assumptions behind such retrievals are not valid close to the equator as the Coriolis parameter tends towards zero. CLS/AVISO has collated and processed altimeter data from all missions since 1992, and they provided weekly gridded estimates of the ocean geostrophic current on a 0.25° × 0.25° grid (Le Traon et al., 1998; Le Traon and Ogor, 1998). The processing by CLS has already involved considerable quality control of the data, so no further editing or filtering was needed. These weekly values were converted to total kinetic energy (TKE i.e. incorporating mean flow plus eddy kinetic energy) and aggregated into monthly products. Maps of TKE (not shown) are marked by intense values at the locations of the strongest currents (especially WBCs and equatorial region), with low values for large expanses of central Atlantic. To calculate an indicator of the province interannual variation for each calendar month, the standard deviation of the TKE was calculated for each pixel. The mean of this standard deviation was then calculated across the province.

4.2. Primary production

Primary Production (PP) was estimated using a primary-production model (Longhurst et al., 1995; Platt and

Please cite this article in press as: Smyth, T., et al. Determining Atlantic Ocean province contrasts and variations. Prog. Oceanogr. (2017), http://dx.doi.org/10.1016/j.pocean.2016.12.004

Sathyendranath, 1988; Platt et al., 1995; Sathyendranath et al., 1995), a combination of remotely-sensed chlorophyll and light data, and information derived from ship-based *in situ* measurements on some model parameters. In validation exercises (comparison with field measurements of primary production), the model compared favourably with respect to other models (Friedrichs et al., 2009; Saba et al., 2011, 2009). For the PP computations, the model parameters related to photosynthetic response to available light and to vertical structure in chlorophyll concentration, were assigned by season and ecological province, as in Longhurst et al. (1995). Each biogeochemical province was assigned five parameters, which varied across four seasons. Two of these were parameters defining the phytoplankton photophysiology: maximum photosynthetic rate per unit chlorophyll concentration at high light levels (P^B_m) and rate of change of production with light availability, when light levels are low (α^B); three parameters were related to the vertical distribution of chlorophyll: the depth of maximum chlorophyll concentration (Z_m), the thickness of the subsurface peak in chlorophyll concentration (σ) and the ratio of the peak chlorophyll concentration to the background chlorophyll concentration (ρ).

The chlorophyll profile parameters were used in conjunction with the remotely-sensed chlorophyll data from the OC-CCI project (version 1.0 data, re-mapped to 9 km resolution), to create chlorophyll profiles for each 9 km pixel. Average sea-surface irradiance (Photosynthetically Active Radiation) for each month and for each location was obtained from NASA and was used to scale the results of a spectral clear-sky model to allow input of spectrally-resolved irradiance into the primary-production model. The propagation of spectral light to various depths in the water column accounted for attenuation by water, phytoplankton and other coloured substances. The profile of light was then combined with the vertical profile of chlorophyll and photosynthetic parameters to obtain estimates of depth-resolved primary production. The calculations were repeated for hourly time steps during the day. The results were then integrated over time and depth to yield total primary production per unit area. Monthly climatologies were produced for the period 1998–2007, which covers the operational lifetime of SeaWiFS.

The quality control of the PP fields is critically dependent upon the quality control of the input fields. The province based parameter assignment should ensure mitigation against anomalous extreme PP values being generated (as the values are broad regional averages). The input PAR fields are quality controlled by NASA and the OC-CCI project has carried out extensive quality assurance of the Chlorophyll product (http://www.esa-oceancolour-cci.org/). Finally the globally integrated PP values were found to agree well with previous estimates of between 40 and 60 GT C yr^{-1} (Carr et al., 2006). It should be noted here that these PP satellite products have not been specifically validated or developed using AMT datasets. For a discussion of alternative approaches see Tilstone et al. (2009).

In order to determine the typical variation in PP, the standard deviation was calculated for each climatological month on a pixel-by-pixel basis. The mean of this standard deviation was then calculated across the province.

5. *In situ* data

5.1. Temperature and salinity

Temperature and salinity depth profiles were measured using electronic Conductivity Temperature Depth (CTD) instruments attached to an oceanographic rosette sampler. Throughout the series, as technology has advanced, the specific model and make of the CTD has changed over time. The CTD profiles were processed according to the cruise reports for cruises AMT1-11. CTDs from cruises AMT12-17 and AMT20 onwards have been processed following standard Sea-Bird protocols using Sea-Bird software. The CTD profiles from AMTs 18 and 19 were carried out using the National Oceanography Centre Southampton PSTAR processing routines. Salinity values using CTD were checked against *in situ* discrete samples taken for analysis on board ship. Approximately 1500 vertical profiles of CTD are available from the twenty-five AMT transects. The resulting temperature and salinity (TS) pairs have been plotted on a graph, for each season (spring, autumn) and province, showing thermosteric anomaly isopleths (Montgomery and Wooster, 1954). The thermosteric anomaly is defined as the specific-volume anomaly for a given salinity and temperature at a standard pressure. It can best be described as bringing a parcel of water at depth, without changing its temperature or salinity, to the surface and calculating the change in the volume due to the change in pressure alone. The data used to construct the isopleths were calculated by varying the temperature and salinity between 0–30 °C and 32–39 PSU respectively at 0.1 unit increments to determine the density (σ). The following formula was then used:

$$\Delta_{S,T} = 1e^{-5} \cdot \left(\frac{1000.}{1000. + \sigma} - 0.97266 \right) \quad (1)$$

and plotted using an isopleth interval of 100×10^{-8} m^3 kg^{-1}. The advantage of overplotting TS pairs on thermosteric anomalies, is that it distinguishes different water masses and their relative stabilities, by the angle at which they follow or cut across the isopleths. For each province a mean TS "profile" was determined by varying the temperature between 2 and 32 °C at 0.1 °C interval bins. For each temperature interval bin the mean temperature and salinity was calculated.

5.2. Oxygen concentration

Vertical profiles of oxygen concentration (μM) were determined using an optode attached to the oceanographic rosette sampler. Profiles are available from AMT12 (2003) onwards. These were calibrated against discrete samples which were analysed for dissolved oxygen concentration using an automated Winkler titration system with a photometric endpoint (Williams and Jenkinson, 1982). Once all of the profiles had been assigned to a Longhurst province, a mean vertical oxygen profile was constructed at 1 m depth intervals, one for each province and season.

5.3. Fluorometric chlorophyll-a

Depth profiles of chlorophyll concentration (mg m^{-3}) were determined using a fluorometer attached to the rosette sampler from AMT10 (2000) onwards. The fluorometer was calibrated against discrete 100 mL seawater samples throughout each individual cruise at multiple depths. These were then filtered through 25 mm GF/F filters, or 0.2 μm polycarbonate filters later in the series, in triplicate and the chlorophyll-*a* extracted in 90% acetone overnight at 4 °C. These filters were then analysed on a Turner fluorometer according to Welschmeyer (1994). The changing shape of the chlorophyll depth profile is indicative of the type of ocean province. The gyral provinces of NATR and SATL are generally characterised by a deep chlorophyll maximum (<0.1 mg m^{-3} typical depth of 70–150 m) with very low surface chlorophyll (<0.03 mg m^{-3}). The mid-latitude provinces (NADR, SSTC) have much higher values of chlorophyll (>0.5 mg m^{-3}) and if present, a subsurface chlorophyll maximum within the top 50 m (mixed layer). Therefore, in order to capture the characteristic shape, each individual depth profile was normalised to its maximum

Please cite this article in press as: Smyth, T., et al. Determining Atlantic Ocean province contrasts and variations. Prog. Oceanogr. (2017), http://dx.doi.org/10.1016/j.pocean.2016.12.004

chlorophyll value and assigned to a particular Longhurst province. This enabled a mean (with associated standard deviation) normalised chlorophyll profile to be constructed at 1 m depth intervals for each province. This approach maintains the shape of the chlorophyll profile and overcomes the issue of chlorophyll ranging over two – three orders of magnitude with depth and latitude. It also enables a solution to the multiple problems which often beset the determination of chlorophyll concentration using fluorometry such as near-surface (high-light) quenching and changes to the calibration "constants" due to changes in phytoplankton community structure (Hemsley et al., 2015).

5.4. Inorganic nutrients

Depth-resolved profiles of inorganic nutrients (nitrate, nitrite, phosphate, silicate) were taken on all AMT cruises except AMT07-09. In this paper we use all the available data until AMT22 (2012). Nutrient samples were collected from Niskin bottles which were triggered at multiple depths throughout the water column (typically all within the top 500 m). Each 60 mL sampling bottle was rinsed three times in seawater from the Niskin before collecting the sample for analysis: non-nitrile gloves were used where possible. All nutrient concentrations were determined using recognised analytical techniques (Woodward and Rees, 2002) as follows: phosphate (Kirkwood, 1989; Zhang and Chi, 2002); silicate (Kirkwood, 1989); nitrate and nitrite ions (Brewer and Riley, 1965); and nitrite analysis (Grasshoff, 1976). Nitrate concentrations were calculated by subtracting the nitrite from the combined nitrate plus nitrite concentration. The nutrients for AMT are sampled and analysed where possible according to GO-SHIP protocols (Hydes et al., 2010), using well tested and developed analytical methods. To ensure quality control Nutrient reference materials are run daily (KANSO, Japan) alongside the samples. The calculated results for the water column and samples are then compared directly against the reference material 'correct' values to ensure the results are within the recommended 2% error of the published reference material results. Corrections can then be made during post cruise data handling and quality control if the results come outside that error window. There has been a consistent methodology of data work-up and quality control from the beginning of the AMT programme to the present day.

On some cruises (AMT12–18), nanomolar nutrient measurements and analyses have been carried out, but they were not included in this paper as they form only six of the possible 25 cruise datasets. The reader is referred to Moore et al. (2009) for a discussion on nanomolar nutrient concentrations along some parts of the transect, as well as Schlosser et al. (2014) who present results of nanomolar phosphate concentration from AMT17 across the "biogeochemical divide" between the north and south Atlantic, which they attribute to seasonal movement of the Intertropical Convergence Zone (ITCZ).

In this paper, data analysis on a by-province basis was carried out to calculate stoichiometric ratios of nitrate:phosphate and nitrate:silicate.

5.5. Flow cytometry

Depth-resolved profiles of picophytoplankton quantified by flow cytometry were acquired on AMT03 and AMT06 and then all subsequent cruises from AMT12 onwards. Seawater samples for enumeration of phytoplankton were collected from predawn and solar noon CTD casts from Niskin bottles attached to the oceanographic rosette sampler into clean 250 mL polycarbonate bottles (Nalge Company, USA) from all depths down to 200 m. The samples were then stored at 4 °C in the dark until analysed (within 2 h). Nano- and picoeukaryote phytoplankton cells were enumerated using a Becton Dickinson FACSort™flow cytometer according to Tarran et al. (2006). Within the analysis window it was possible to resolve three groups of picophytoplankton: *Prochlorococcus* sp. and *Synechococcus* sp. (cyanobacteria) and picoeukaryotic phytoplankton. In addition, three groupings of nanophyoplankton were resolved: coccolithophores (coccolith-bearing, 5–8 μm), cryptophytes and other nanophytoplankton.

5.6. Phytoplankton pigments

For the determination of pigments: between 1 L and 4 L of seawater was filtered onto a Whatman® GF/F glass microfibre filter and the filter stored in liquid nitrogen until analysis. If liquid nitrogen was not available the filters were stored in a −80 °C freezer. For the analysis stage, pigments were extracted from the thawed GF/F filter under dim light conditions on ice, in 2 mL 90% acetone by sonication (Sonics Vibracell probe, 35 s, 40 W), followed by a soaking period (total extraction time = 1 h). Extracts were clarified by centrifugation. For analysis details of samples from AMT01-17 see Aiken et al. (2009). Samples from AMT18-20 were analysed on an Accela HPLC instrument (ThermoFisherScientific) comprising an Accela quarternary pump, thermostated autosampler, thermostated column compartment and photodiode array detector using a method based on Barlow et al. (1997). Samples from AMT21 onwards were also analysed using an Accela instrument, but the method of Zapata et al. (2000) was applied, with minor modifications (Steele et al., 2015). Samples were analysed within 24 h of extraction during which time they were maintained at 4 °C in the dark in the autosampler. Pigments, including chlorophyll-*a*, were identified using retention time and spectrally matched using photo-diode array spectroscopy (Jeffrey and Wright, 1997). Pigment concentrations were determined by response factors, generated at the time of instrument calibration. Multipoint calibration of 19 pigments is performed annually by injection of pigments standards obtained from the DHI institute for Water and Environment, Denmark. For calibration curves, the standards were used to prepare a dilution series, comprising three solutions bracketing the limit of quantification (LOQ), and three bracketing the expected sample concentration. For data analysis, the ratio of photosynthetic pigments (*Total Chlorophyll, 19′-Butanoloxyfucoxanthin, Fucoxanthin, 19′-Hexanoloxyfucoxanthin, Peridinin*) to photoprotective carotenoids (*Alloxanthin, Diadinoxanthin, Diatoxanthin, Zeaxanthin, carotenes*) was calculated after each sample had been assigned to a Longhurst province.

Finally, fractions of pico- (cells <2 μm), nano- (cells 2–20 μm) and microphytoplankton (cells >20 μm) to total chlorophyll were computed from key diagnostic pigments following Uitz et al. (2006) as modified by Brewin et al. (2010), and averaged for each province and each season, together with chlorophyll concentrations averaged in $\log_{10}$-space (Campbell, 1995).

HPLC data was available for all AMT cruises except for AMT09: in this paper we use data from AMT01–23.

5.7. Optical Plankton Counter

Samples for mesozooplankton were taken using pre-dawn vertical net hauls on AMT01-12 and 18–22. A double (bongo) net frame was deployed, with 0.57 m diameter openings and carrying two WP2 nets with 200 μm nylon mesh, fitted with cod ends with 200 μm mesh windows. The net samples were run through an Optical Plankton Counter (OPC). The OPC is capable of reliable and rapid characterization of marine zooplankton populations between 0.25 and 16 mm equivalent spherical diameter (ESD, Herman (1992)) in up to 4096 size classes and at data rates of up to 200 events s^{-1}. The OPC measures cross-sectional area of each particle passing between a collimated rectangular beam of red

Please cite this article in press as: Smyth, T., et al. Determining Atlantic Ocean province contrasts and variations. Prog. Oceanogr. (2017), http://dx.doi.org/10.1016/j.pocean.2016.12.004

light and a rectangular light sensor as digital size. This digital size is converted to ESD using a semi-empirical formula, representing the diameter of a spherical particle presenting the same cross-sectional area as that detected for the particle.

For graphical representations of individual AMT transect section variables, the reader is directed towards the individual cruise reports (www.amt-uk.org/Cruises) and the three previous AMT special issue collections (Aiken and Bale, 2000; Robinson et al., 2006, 2009).

6. Results and discussion

6.1. Physical drivers

6.1.1. Heat flux

February and August have been selected in Fig. 2 to maximise the hemispherical contrasts: there is little difference in the heat flux fields when comparing the two equinoxial periods. The dominant component is the SW term which reaches values between 250 and 300 W m^{-2} in the tropical summer and varies seasonally between 50 and 150 W m^{-2} in the mid-latitudes. The LH is the next most dominant flux term and is particularly marked in the tropics (150–200 W m^{-2}) and the winter Gulf Stream (250–300 W m^{-2}), which also is distinctive in the SH flux (75 W m^{-2}). All four of these components result in the NH flux, with strong seasonal and hemispheric heterogeneities. The boreal winter is dominated by a large NH flux out of the water column (200 W m^{-2}) with strong latitudinal gradients, particularly around the Gulf Stream. The austral summer is characterised by weaker gradients but an overall NH flux into the water column. The reverse is true in the boreal summer/austral winter, as should be expected for a system dominated by the solar input of shortwave radiation.

As with the absolute values of the heat flux components, there are strong seasonal variations in the standard deviation of the NH flux (Fig. 3): the peak in the variation in the northern hemisphere provinces is in January or February (Fig. 4a). For the southern hemisphere provinces the peak variation is in July (SATL) or August (SSTC). The maximum variation in this analysis is in the NADR province (53 W m^{-2} in February), whereas the smallest amount of variation is in the WTRA (15–22 W m^{-2}) over the annual cycle. The NADR variation is likely driven by fluctuations in the position of the Gulf Stream, which would govern SH and LH fluxes, and inherent variation in weather systems which would additionally affect SW and LW fluxes. The WTRA is subject to the smallest amount of seasonality in the dominant SW flux. All three northern hemisphere provinces converge towards 15–20 W m^{-2} variation in the months May–August. This is generally when the most settled atmospheric conditions occur. They then diverge in September as the mid-latitude weather systems begin to intensify in the autumn.

6.1.2. Ocean currents – TKE

Four of the six provinces under investigation (NADR, NASE, NATR and SATL) show little annual average variation in TKE (Fig. 4b). The least variation is in the NATR province (75–95 cm^2 s^{-2}). This is due to the location of this province in the centre of the north Atlantic gyre and away from the dynamic processes at the eastern boundaries. The variation that there is will be driven by eddies which periodically traverse the gyres, generated at their extremities. The southern gyre (SATL) seems to be more dynamically variable than the northern gyre (113–129 cm^2 s^{-2}). This is probably due to the southern boundary of the gyre being driven by the highly dynamic Southern Ocean (south of the SSTC which has a factor of two more variation). The gyre is also flanked to the west by the Brazillian current and to the east by the Benguela upwelling. The greatest amount of annual variation is encountered in the WTRA (220–440 cm^2 s^{-2}). This province is dominated by the equatorial upwelling and associated currents, although as noted earlier, many of the assumptions required in generating these fields of TKE, collapse at the equator.

6.2. Observed responses: Satellite

6.2.1. Primary production

The mid- to high-latitudes are characterised by the largest variation in PP (Fig. 5), which is at a minimum in the winter and a maximum in the spring and summer when episodic phytoplankton blooms and their associated succession occur. The gyres also demonstrate seasonality but to a lesser extent. Not only is the magnitude of the peak in PP variation modulated by latitude, but also its timing (Fig. 4c). The peak in PP variation occurs in May in the NADR (270 mg C m^{-2} d^{-1}) and April in the NASE (116 mg C m^{-2} d^{-1}), July in the NATR and August in the WTRA. For both southern hemisphere provinces the peak in PP variation occurs in November (150 mg C m^{-2} d^{-1} and 40 mg C m^{-2} d^{-1} for the SSTC and SATL respectively). This confirms that, for four out of the six provinces, AMT occurs during the months of greatest change (in this case, PP).

6.2.2. Observed responses: In situ

The southbound cruises which commence during the boreal autumn (austral spring) have been nominally labelled as October, although the cruise duration is generally September–November. The northbound cruises which commence during the austral autumn (boreal spring) have been similarly labelled as April, although the cruises may be April–June.

6.2.3. Temperature, salinity profiles

General seasonal patterns can be observed in Fig. 6: the boreal NADR, NASE and NATR are markedly warmer (2–4 °C), and in some cases more saline in October than in April. The reverse is true in the SATL and SSTC with the least variation in temperature occurring in the WTRA province. The tropical provinces of the NATR, WTRA and SATL show large variations in the surface salinity fields. Variations in the near surface salinity is driven by the balance between precipitation and evaporation: this balance is altered as the Inter Tropical Convergence Zone, characterised by heavy convective rainfall, tracks northwards and southwards through these provinces, lagging the sun by approximately six weeks. The highest salinities (>37) are encountered in the (northernmost) NATR during October, which is the region least affected by surface precipitation. The lowest surface salinities (<34) are observed in the WTRA which experiences a double crossing of the ITCZ and hence two periods of enhanced precipitation. This province may also be affected by the Amazon freshwater outflow (Hooker et al., 2000).

Different water masses through the water column can be clearly seen, the boundaries marked by changes in the density gradient (TS slope). The NATR in October for example, is described by four different water masses: (1) Antarctic Intermediate Water (AAIW) for temperatures <4 °C and salinities between 34 and 35; (2) lower North Atlantic Central Water (lNACW) for the dominant part of the profile (4 °C < T < 22 °C); (3) upper North Atlantic Central Water (uNACW) above this (22 °C < T < 27 °C) and; (4) a seasonally variable surface mixed layer which is strongly modulated by latitudinal position, turbulent processes (heat flux, wind) and precipitation. Typical CTD casts on AMT generally observe the top 200–500 m of the water column. However, the occasional deeper cast (2000–5000 m) encounters the exotic AAIW in the tropical provinces (NATR, WTRA and SATL). The dominant water mass in the SATL province is South Atlantic Central Water (SACW) between 4 °C < T < 25 °C in October, and 23 °C in April. The difference in the position of the isopycnal may be more driven by the location of

Please cite this article in press as: Smyth, T., et al. Determining Atlantic Ocean province contrasts and variations. Prog. Oceanogr. (2017), http://dx.doi.org/10.1016/j.pocean.2016.12.004

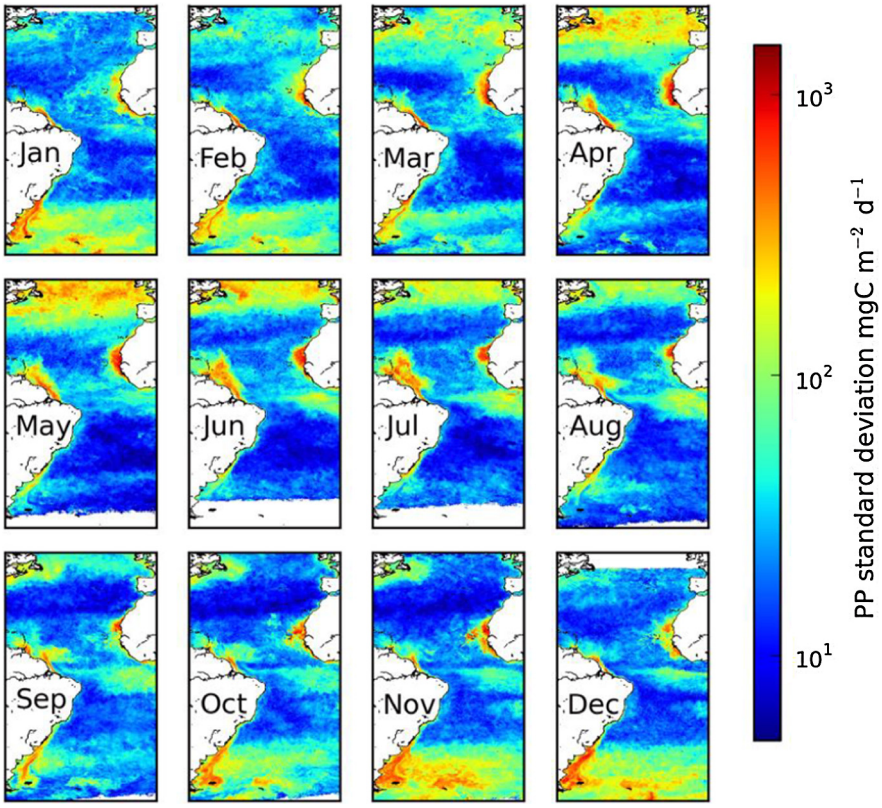

Fig. 5. Standard deviation in monthly primary production (PP-mg C m^{-2} d^{-1}) derived using EO data. (See web version of this article for colour.)

the cruise as some northbound AMTs were on the eastern side of the Atlantic rather than the west. Seasonal surface mixed layers, strongly modulated by the connection to the atmosphere are apparent in the top part of the water column in all the tropical provinces (NATR, WTRA and SATL). This is shown by the differences between the plots for April and October as well as variation (data spread) within the top mixed layer. In a seeming dichotomy though, these layers are highly stable as shown by the marked inflexion towards a negative gradient in TS space in the median profile. This crosses the thermosteric anomaly contours at right angles in some cases, the surface sea-water in these locations being less dense by virtue of being both warmer and fresher than the underlying layers. Of the tropical provinces the surface stability is strongest in the NATR and weakest in the SATL but seasonal aliasing may be skewing this picture: more cruises have occurred in the boreal autumn/austral spring (17) than vice versa (8). The SATL on the majority of cruises has been sampled in the period emerging from the winter and therefore, the surface thermocline is not as well developed. This sample skewing towards October results in a higher number of TS pairs (SATL: October N = 172,658; April N = 58,686).

6.2.4. Oxygen

The mid-latitude provinces in both hemispheres (NADR, SSTC) show little variation in oxygen (Fig. 7) with a range of 220–260 μM observed throughout the depths sampled. There is also only a small amount of seasonal variation, this being driven by temperature with the cooler season having the highest concentrations of dissolved oxygen. The biologically net autotrophic component of the signal resides within the top 50 m of the water column. A subsurface oxygen maximum of 220 μM is present at around 60 m in the autumn NASE province. The other tropical provinces (NATR, WTRA) are dominated by strong subsurface reductions in oxygen. The oxycline is closest to the surface in the autumn NATR province and most intense in the WTRA province, with concentrations as low as 50 μM around (and below) 300 m. This oxygen minimum zone (OMZ) in the tropical Atlantic is well documented (Karstensen et al., 2008) and is a result of large-scale circulation patterns causing weak ocean ventilation. The SATL province, situated in the southern gyre, has an observable OMZ in some profiles, however it is lower in the water column (oxycline below 120 m) and less intense with values not below 80 μM.

Ventilation of the OMZ in the tropical north Atlantic is not primarily driven by local air-sea interactions and subsequent diapycnal mixing (i.e. across density gradients) from directly above, but through isopycnal transport (i.e. along density gradients) of water masses and their corresponding dissolved oxygen concentrations. The strength of the oxygen minimum in the subsurface is a function of both the export of organic material from above and the ventilation of the thermocline through physical processes. The lower oxygen within the OMZ on the eastern, compared with the western, side of the Atlantic gyre systems is a function of both increased export of organic material from the eastern boundary current upwelling systems and the lower ventilation rates of the thermocline on the eastern side.

Although documenting how OMZs of the Atlantic have changed (or indeed vary) over time is difficult because of longitudinal and aliasing within the AMT dataset, the values presented here should be considered as representative of each of the provinces investigated. Stramma et al. (2008) using a time-series of historical data augmented with meridional hydrographic sections along 29°W (July 2003) and 23°W (July 2006) showed an oxygen decrease in the oxygen-poor region of the tropical North Atlantic (equivalent to the NATR) of 0.34 μM yr^{-1} since 1960. Within the NATR OMZ the oxygen values have declined and the OMZ has expanded vertically over that time period (Stramma et al., 2008).

Please cite this article in press as: Smyth, T., et al. Determining Atlantic Ocean province contrasts and variations. Prog. Oceanogr. (2017), http://dx.doi.org/10.1016/j.pocean.2016.12.004

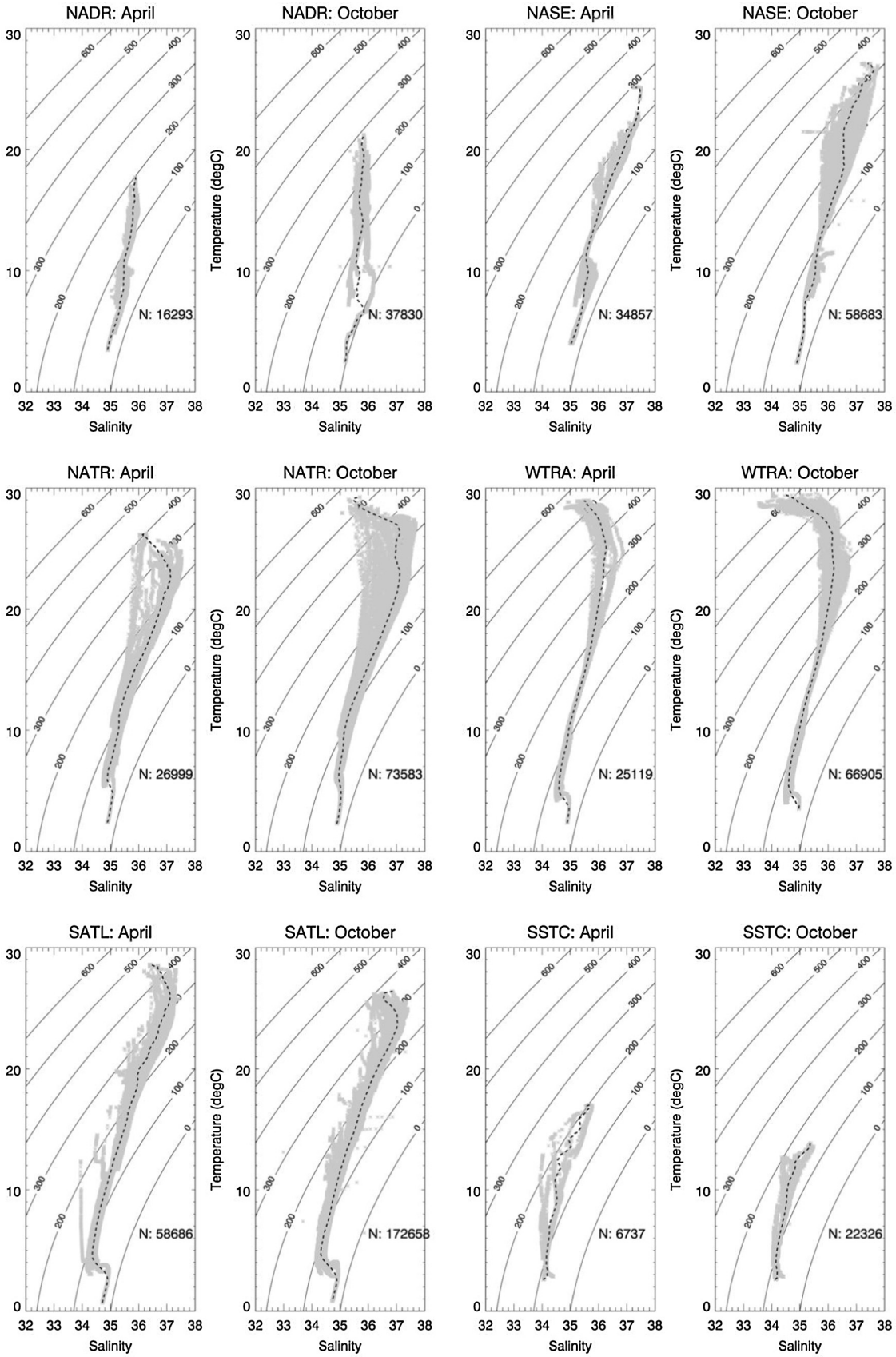

Fig. 6. Temperature-salinity (TS) plots annotated with contours of constant thermosteric anomaly (10^{-8} m^3 kg^{-1}) for six Longhurst provinces, separated into the different cruise seasons (April, October). Dashed line represents a mean T,S "profile".

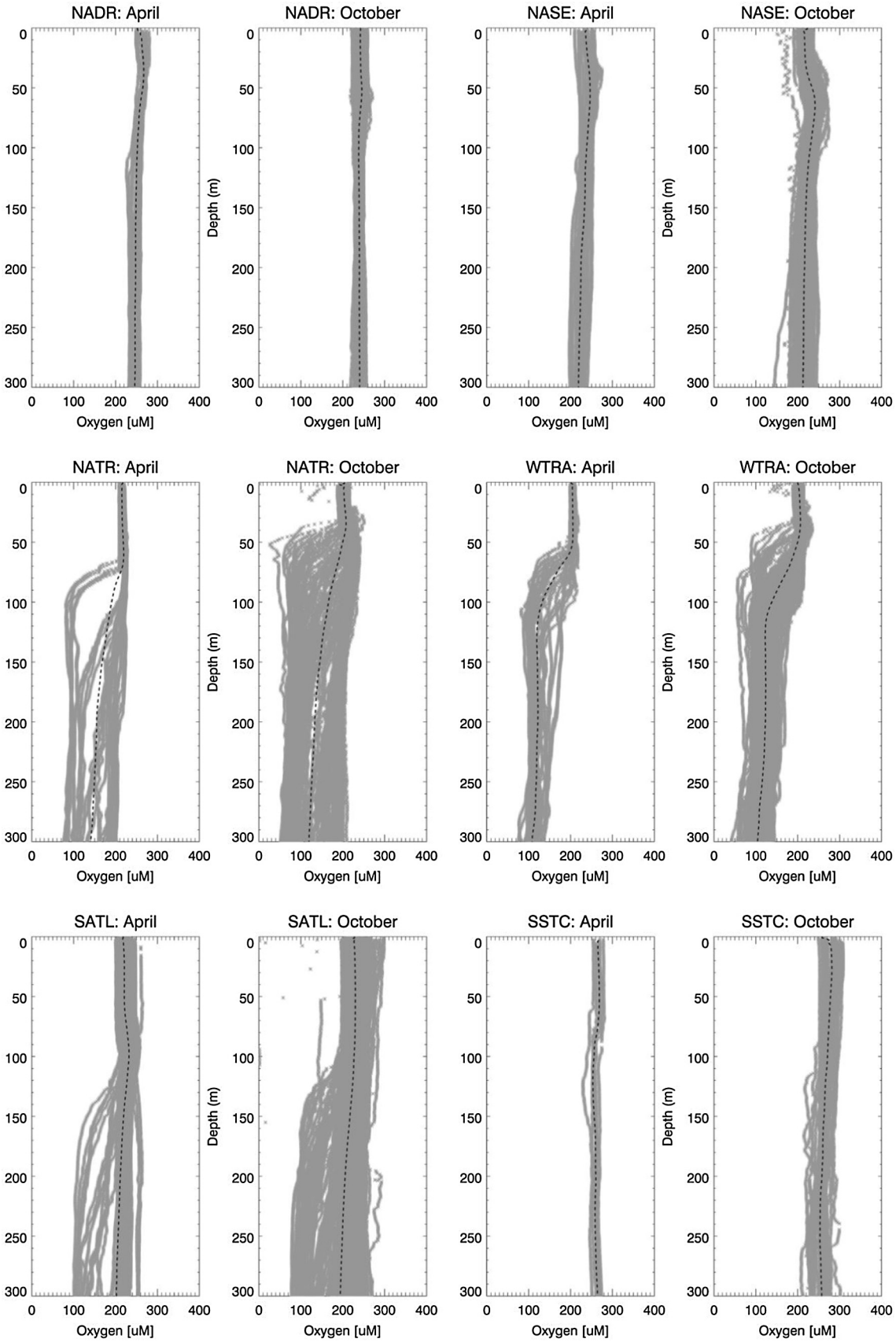

Fig. 7. Vertical profiles of oxygen concentration for six Longhurst provinces, separated into the different cruise seasons (April, October). Dashed line represents the mean vertical oxygen profile.

6.2.5. Chlorophyll fluorescence

The location of the normalised maximum in chlorophyll fluorescence (Fig. 8) is within the surface mixed layer for the mid-latitude provinces of the NADR and SSTC. Particularly in April for the SSTC province, the chlorophyll is relatively homogeneous in the surface mixed layer down to a depth of 60 m, rapidly dropping off below this to give chlorophyll values around an order of magnitude lower. This is broadly repeated for these two provinces with nuances in the seasonality. Within all the tropical provinces (NASE, NATR, WTRA, SATL) a deep-chlorophyll maximum (DCM) exists, whose depth location and magnitude is governed by the seasons. All these provinces are characterised by a shoaling of the chlorophyll maximum between the spring and autumn seasons which is likely to be strongly connected to the shoaling of the mixed layer depth in those months. For example, the SATL chlorophyll maximum shoals from 136 m in October (spring) to 115 m in April (autumn) whereas in the NATR the DCM shoals from 107 m in April (spring) to 70 m October (autumn). The equatorial province of WTRA has a well-marked DCM in both seasons with only slight variations in depth (66–77 m). The least marked, in terms of relative gradients with depth is in the October SATL, with only a doubling of chlorophyll between the surface and 136 m. The closer that the relative chlorophyll at the DCM is to unity, the less variation on a vertical profile-to-profile basis there is within the province in terms of the depth of the DCM. For example, the SSTC province in April has a relative value of 0.97 in the surface mixed layer indicating that the chlorophyll maximum is consistently to be found within this narrow region. By contrast the SATL province in October has a normalised peak chlorophyll value of 0.34, indicating a broader spread of depths which the DCM is to be found within this province. However, this needs to be interpreted with caution as there are 145,846 data points for the latter, and 5329 for the former. This is as a result of more cruise tracks covering the SATL province than any other and also its large size. The tropical provinces are all characterised by small differences between the maximum and minimum chlorophyll encountered within the euphotic zone. This ranges between a factor of 5 (NATR: April) and 11 (NASE: October). Greater variation is shown in the mid-latitude provinces ranging between 9 (SSTC: April), 22 (NADR: April), 25 (NADR: October) and 35 (SSTC: October).

Analysing the relative chlorophyll (Fig. 8) in conjunction with the oxygen profiles (Figs. 7 and 8 for a comparison with the normalised mean oxygen profile) shows that the oxygen maximum is situated at or slightly below the sub-surface chlorophyll maximum in the mid-latitude provinces (NADR, SSTC) whereas in the tropical provinces the oxygen maximum is located above the chlorophyll maximum. Typical separations between the DCM and the oxygen maximum range between +13 m (NASE: April) and +87 m (SATL: October). The position of the oxygen maximum also varies with season, shoaling in phase with the DCM in these provinces, apart from in the SATL during October. This suggests that there is a strong and relatively rapid connection between the oxygen concentration and biological activity in the mid-latitudes. In the tropics, the DCM is situated within the top layer of the OMZ which complicates the attribution of the signal because of the dominance of large scale physical circulation patterns. However, it would seem that there is still a biological signal within the oxygen profiles as both maxima (chlorophyll, oxygen) are broadly in phase seasonally. In the gyres the productivity maximum is above the DCM as productivity is also a function of irradiance (as well as chlorophyll, temperature (Morel, 1991) and nutrient availability). Therefore, despite lower concentrations of chlorophyll above the DCM, productivity is greater due to the higher light levels. This is because DCM does not really reflect productivity but rather a community of high chlorophyll:carbon ratio phytoplankton adapted to low light.

6.2.6. Nutrients

Within all of the provinces there is a tendency towards the Redfield (1958) ratio deeper in the water column especially at depths >150 m (Fig. 9). As has been observed previously (Moore et al., 2009, 2013; Tyrrell, 1999) there is an excess (i.e. above Redfield) in phosphate at low nitrate concentrations. The deviation from the 16:1 N:P ratio occurs roughly when the nitrate concentration is below 5 μM in the NADR province but as high as 20 μM in the SATL. This hemispherical difference has been observed previously (Deutsch et al., 2007; Gruber and Sarmiento, 1997; Moore et al., 2013) and attributed to iron limitation, as nitrogen fixation as a source of additional nitrogen, is an iron intensive process. The theory is that the northern gyre (NATR) is not iron limited due to periodic inputs of Saharan dust transported and deposited into the ocean via strong winds. These episodic inputs of iron enhance nitrogen fixation by diazotrophic cyanobacteria, including *Trichodesmium*. This is in contrast to the southern gyre (SATL) which has no such ready source of terrestrial iron. It is also worth noting that atmospheric fixed nitrogen deposition may also be significant, with the northern gyre being closer to anthropogenic sources in North America and Europe (Zamora et al., 2010).

The solid line curves in Fig. 9 are a second order polynomial log-fit with the constants shown in Table 1. These can be used to predict a concentration of phosphate for a given value of nitrate. For example, in the NATR for a nitrate concentration of 0.6 μM the phosphate concentration is predicted to be 0.07 μM (N:P = 0.12). By contrast in the SATL the phosphate concentration is predicted to be 0.2 μM (N:P = 0.33). These results clearly show the difference in phosphate between the two gyres that AMT has played a major part in revealing.

The top 50 m of the water column are characterised by diminishing nitrate and phosphate as this is where phytoplankton exhaust these nutrients most rapidly. This becomes particularly acute in the tropical provinces of NASE, NATR and SATL where nitrate drops below the limit of detection (<0.03 μM) in the surface layer. The equatorial upwelling region, within the WTRA province, shows elevated concentrations of both nitrate and phosphate in the surface (0–50 m) layer when compared with the provinces immediately to the north (NATR) and south (SATL). The strong dynamics of this narrow equatorial region, where a combination of surface easterly winds and the Coriolis parameter becoming vanishingly small, result in vigorous Ekman pumping, driving cooler, deeper, nutrient-rich waters into the top 50 m of the water column. This in turn drives higher concentrations of chlorophyll and primary production (PP). The literature, however, is somewhat equivocal about this. Longhurst et al. (1995), based on the Coastal Zone Color Scanner (CZCS) satellite mission, estimate the daily averaged PP to be 0.29, 0.36 and 0.21 gC m^{-2} d^{-1} in the NATR, WTRA and SATL provinces respectively. Based on a limited subset of *in situ* data, Tilstone et al. (2009) gave a figure of 0.30, 0.26 and 0.21 gC m^{-2} d^{-1}; whereas implementing the PP model of Smyth et al. (2005) on the SeaWiFS dataset the values were 0.31, 0.35 and 0.26 gC m^{-2} d^{-1} respectively. The differences in these three datasets reflects differences in sampling techniques, input datasets and associated algorithms, data sparsity (in the case of *in situ* and to a lesser extent the CZCS), and spatial-temporal heterogeneity. It is also likely that the narrowness of the equatorial upwelling zone contributes to its effect being diluted in the wider context of the WTRA province as a whole.

The mid-latitude provinces of NADR and SSTC are characterised by seasonal nitrate depletion in the surface layer. The AMT cruise seasonal aliasing can be clearly seen in the difference between these two provinces: NADR is entering into the boreal autumn phase so surface nutrients are at their lowest point before being replenished by winter mixing, whereas the SSTC is just starting

Please cite this article in press as: Smyth, T., et al. Determining Atlantic Ocean province contrasts and variations. Prog. Oceanogr. (2017), http://dx.doi.org/10.1016/j.pocean.2016.12.004

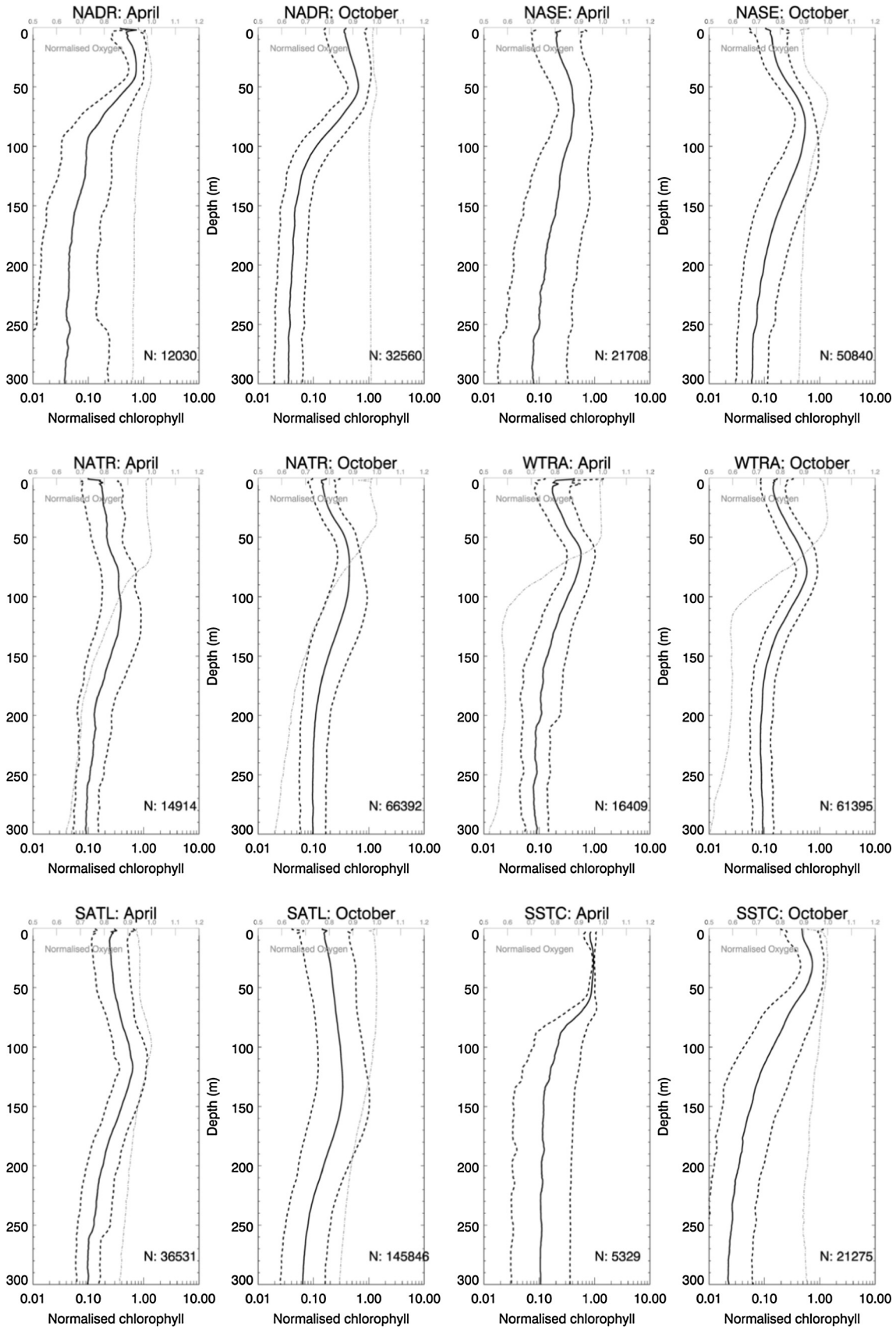

Fig. 8. Mean normalised (to the maximum chlorophyll concentration in each individual profile) chlorophyll determined using a fluorometer (solid line) for six Longhurst provinces, separated into the different cruise seasons (April, October). Dashed line represents one standard deviation; N is the number of samples taken in each province and season to construct the profile. Note log-scale on lower x-axis. The mean normalised oxygen profile (data from Fig. 7) is shown as grey dash-dot line to enable comparisons between the oxygen and chlorophyll profiles to be made. Note linear scale on upper (grey) x-axis.

Please cite this article in press as: Smyth, T., et al. Determining Atlantic Ocean province contrasts and variations. Prog. Oceanogr. (2017), http://dx.doi.org/10.1016/j.pocean.2016.12.004

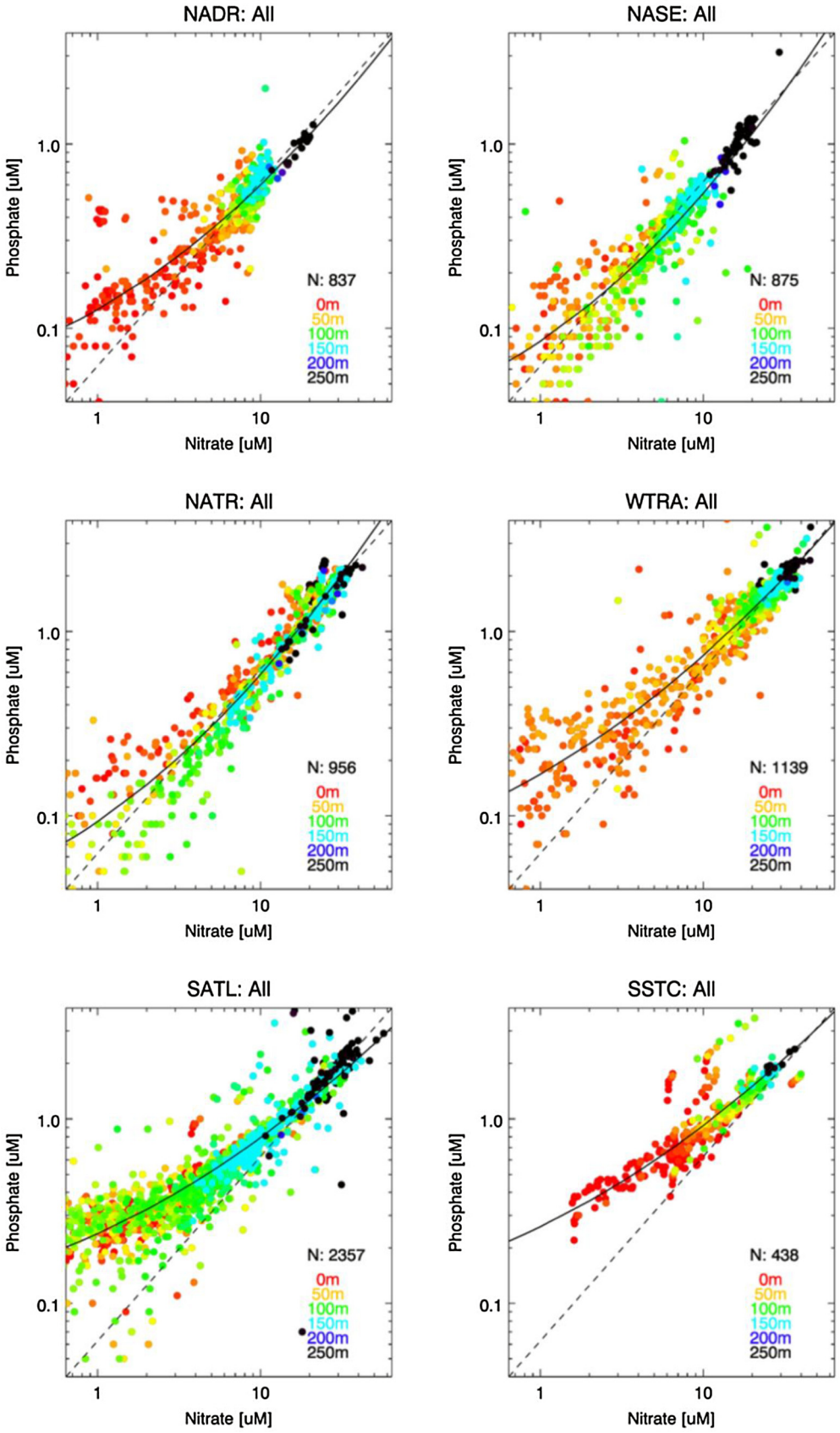

Fig. 9. Phosphate versus nitrate for six Longhurst provinces. All seasons have been amalgamated in these plots. The Redfield ratio of Nitrate:Phosphate 16:1 is shown as a dashed line and the position that the samples were taken in the water column are colour coded. Solid line is the second order polynomial fit, with coefficients given in Table 1. N is the number of samples taken in each province. (For interpretation of the references to colour in this figure legend, the reader is referred to the web version of this article.)

Please cite this article in press as: Smyth, T., et al. Determining Atlantic Ocean province contrasts and variations. Prog. Oceanogr. (2017), http://dx.doi.org/10.1016/j.pocean.2016.12.004

Table 1
Polynomial fit to equation of form log P = A(log N)^2 + B log N + C for six Longhurst provinces with associated regression statistics, where P is phosphate and N nitrate concentration in μM. Data are shown in Fig. 9.

Province	A	B	C	R^2	RMSE
NADR	0.174	0.501	−0.898	0.847	0.185
NASE	0.209	0.593	−1.070	0.874	0.192
NATR	0.194	0.604	−1.031	0.931	0.196
WTRA	0.138	0.506	−0.775	0.800	0.205
SATL	0.123	0.398	−0.622	0.795	0.187
SSTC	0.121	0.427	−0.585	0.549	0.115

the spring bloom where surface nutrients should be at or around their peak concentrations.

The Redfield ratio was extended by Brzezinski (1985) to include silicate. This is because diatoms, which are strongly competitive phytoplankton and contribute significantly to global primary production (Mann, 1999), require silicic acid to create biogenic silica for their cell wall structure. Yool and Tyrrell (2003), expanding on an earlier modelling study (Tyrrell, 1999) into the relative influences of nitrogen and phosphorus on oceanic primary production, investigated the role of diatoms in regulating the ocean's silicon cycle. Their plots of nitrate vs phosphate and silicic acid vs phosphate (Fig. 1 in Yool and Tyrrell (2003)) showed similar behaviour close to the origin. This, they suggested, is due to the controls of competing algal groups and in the case of silicon, caused by diatom activity. Fig. 10 shows similar behaviour in five out of the six provinces studied; the exception being SSTC. Below nitrate concentrations of 1–2 μM in the tropical provinces, the surface waters are characterised by N:Si ratios that deviate below the expanded Redfield ratio (above the dashed line in Fig. 10). This is likely to be a reflection on Si not being drawn down below 1–2 μM while nitrate becomes increasingly exhausted. However, with increasing depth (between 50 and 200 m) there appears to be divergence above the 16:15 nitrate to silicate ratio (below the dashed line in Fig. 10). This is in contrast to the behaviour shown for N:P in Fig. 9 where there is an increasing tendency towards Redfield with depth. Yool and Tyrrell (2003) attributed this difference to active remineralisation processes which strongly couple nitrate and phosphate concentration, whereas biogenic silica dissolution is slower and only weakly coupled to these processes. In the SSTC province there is a lack of surface silicate which may be due to several factors. It may be caused by the colder surface temperatures in this region (5–10 °C): silica dissolution is known to be strongly temperature dependent, with the specific dissolution rate increasing by approximately an order of magnitude with each 15 °C increase in temperature (Kamatani, 1982). It may also be due to surface diatom blooms exhausting the surface silicate concentration as several large diatom blooms have been encountered in this province during the AMT programme (Tarran, *pers. comm.*). Finally it may be caused by this province being remote from terrestrial sources (rivers, dust) of available silicate.

Each of the provinces also need to be interpreted in a three-dimensional sense as some of the changes in the silicate versus nitrate relationship with depth may actually reflect the differences between water masses (Sarmiento et al., 2004). Thus for example, Southern Ocean sourced water masses (Sub-Antarctic Mode Water, AAIW) have relative low Si:N ratios (Palter et al., 2010; Sarmiento et al., 2004) and this may influence the relationships observed in Fig. 10.

The strong relationships between N:P and N:Si and how these relationships differ from province to province gives additional observational evidence when constraining numerical biogeochemical or ecosystem models in the open ocean. As well as confirming the results of (Moore et al., 2009) showing different deviations away from the Redfield ratio in the northern and southern gyres, the data presented in this paper extend the observations temporally and to all the major provinces. It seems that the tendency towards an excess of phosphate in the surface (<150 m) increases with distance south of the equator. The results show a remarkable coherence in stoichiometric relationships, for each province with strong predictive skill (e.g. R^2 between 0.549 and 0.931 for phosphate vs nitrate regressions). Such relationships could be applied to set the limits on emergent biogeochemical properties (de Mora et al., 2016) for example.

Finally it is important to make two additional points. Firstly, Redfield ratios need to be interpreted cautiously because they reflect standing stock not flow rates. Secondly, using such ratios in oligotrophic waters may create anomalies. This will be caused by the different instrumental limits of detection for nitrate and phosphate, which are far from being Redfield. However, the smooth curves showing the evolution of N:P (Fig. 9) over a range of concentrations is reassuring that this artefact has at least been partially ameliorated.

6.2.7. Flow cytometry

There is a clear delimitation between the sub-tropical/tropical (NASE, NATR, WTRA, SATL) and the mid-latitude (NADR, SSTC) provinces in terms of the very small (pico-)plankton (Fig. 11). Both the *Prochlorococcus* (0.6 μm) and *Synechococcus* (0.8–1.5 μm) cyanobacteria are present in all of the provinces, with a concentration range of between 1 and 10^6 mL^{-1}. In the mid-latitude provinces, there is only a weak linear relationship in their relative concentrations: broadly, that as the concentration of *Prochlorococcus* increases so does the concentration of *Synechococcus*. This is most pronounced in the NADR province. *Prochlorococcus* does seem to be present in greater abundance in the SSTC, although this province has considerably fewer samples in comparison with the NADR. The equatorial WTRA province appears to show two well separated patterns. In the surface layer (0–50 m, typical of the surface mixed-layer thickness in this region), there is a strong linear relationship between *Prochlorococcus* and *Synechococcus* abundance. The rise in *Synechococcus* concentration is two orders of magnitude greater than that of *Prochlorococcus*, despite its larger size. Below the surface mixed-layer the abundance of *Synechococcus* appears to be capped below 10^2 mL^{-1}. This general pattern, particularly the linear relationship at higher abundances of *Prochlorococcus*, is replicated in the NASE, NATR and SATL provinces and perhaps could be considered as a measure of oligotrophy. This could also provide a threshold in ecosystem models which describe plankton functional types (Blackford et al., 2004).

In general these province patterns show that there is always competition between *Prochlorococcus* and *Synechococcus*, particularly when considering the scarcity of nutrients in the oligotrophic gyres (NASE, NATR, SATL). *Prochlorococcus* are specialists. They are able to exploit the oligotrophic gyres in general (Zubkov et al., 2003) and low light conditions in particular (i.e. at the DCM (Partensky et al., 1999)) far better than *Synechococcus*, whereas *Synechococcus* thrives better where there are detectable (>0.1 μM nitrate) nutrients. Their main limitation seems to be temperature:

Please cite this article in press as: Smyth, T., et al. Determining Atlantic Ocean province contrasts and variations. Prog. Oceanogr. (2017), http://dx.doi.org/10.1016/j.pocean.2016.12.004

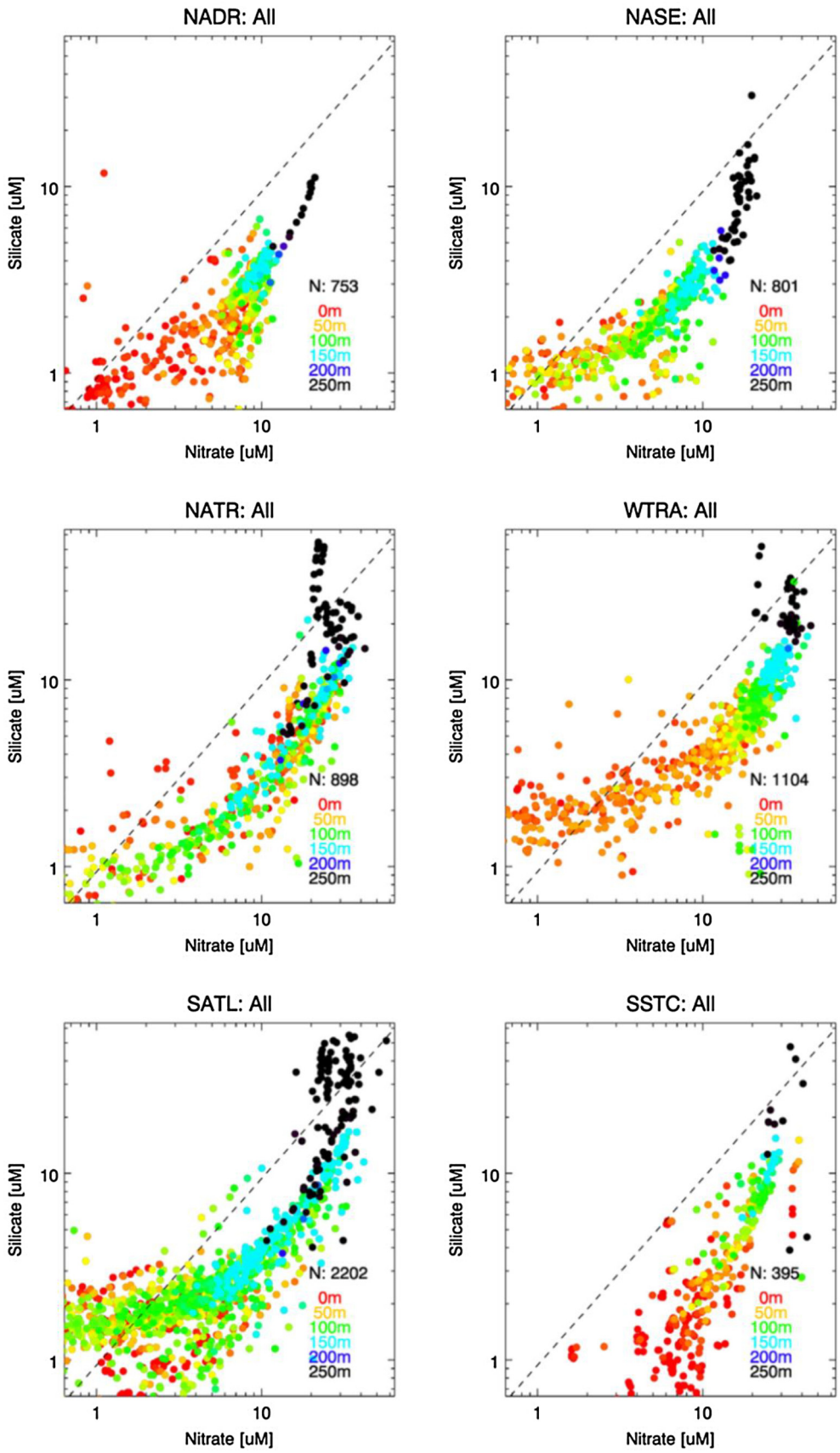

Fig. 10. Silicate versus Nitrate concentration for six Longhurst provinces. All seasons have been amalgamated in these plots. The Redfield ratio of Nitrate:Silicate 16:15 is shown as a dashed line and the position that the samples were taken in the water column is colour coded. N is the number of samples taken in each province. (For interpretation of the references to colour in this figure legend, the reader is referred to the web version of this article.)

Please cite this article in press as: Smyth, T., et al. Determining Atlantic Ocean province contrasts and variations. Prog. Oceanogr. (2017), http://dx.doi.org/10.1016/j.pocean.2016.12.004

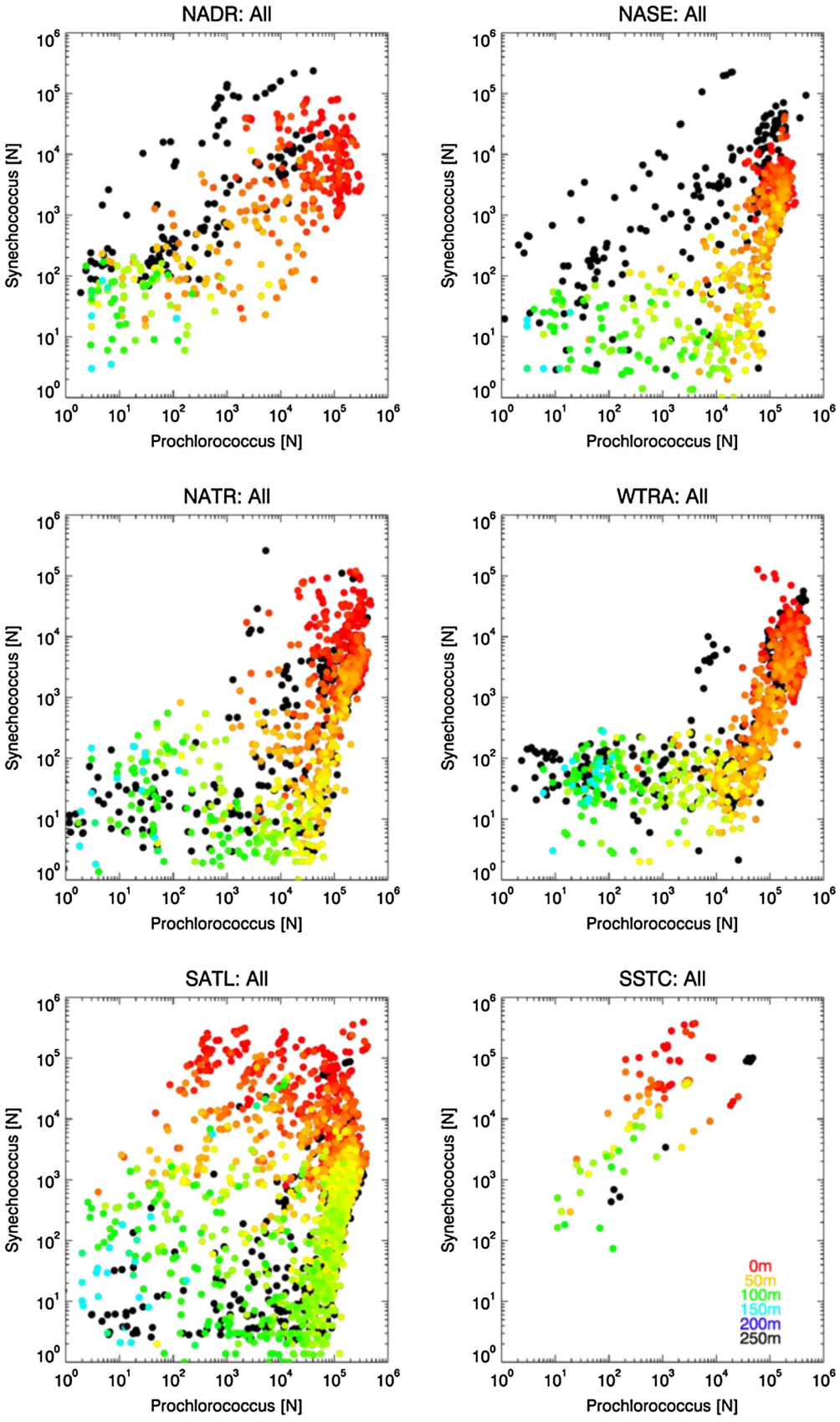

Fig. 11. Abundances of Synechococcus [N] versus Prochlorococcus [N], determined using Flow Cytometry, as a function of depth for six Longhurst provinces. The position that the samples were taken in the water column is colour coded. (For interpretation of the references to colour in this figure legend, the reader is referred to the web version of this article.)

Please cite this article in press as: Smyth, T., et al. Determining Atlantic Ocean province contrasts and variations. Prog. Oceanogr. (2017), http://dx.doi.org/10.1016/j.pocean.2016.12.004

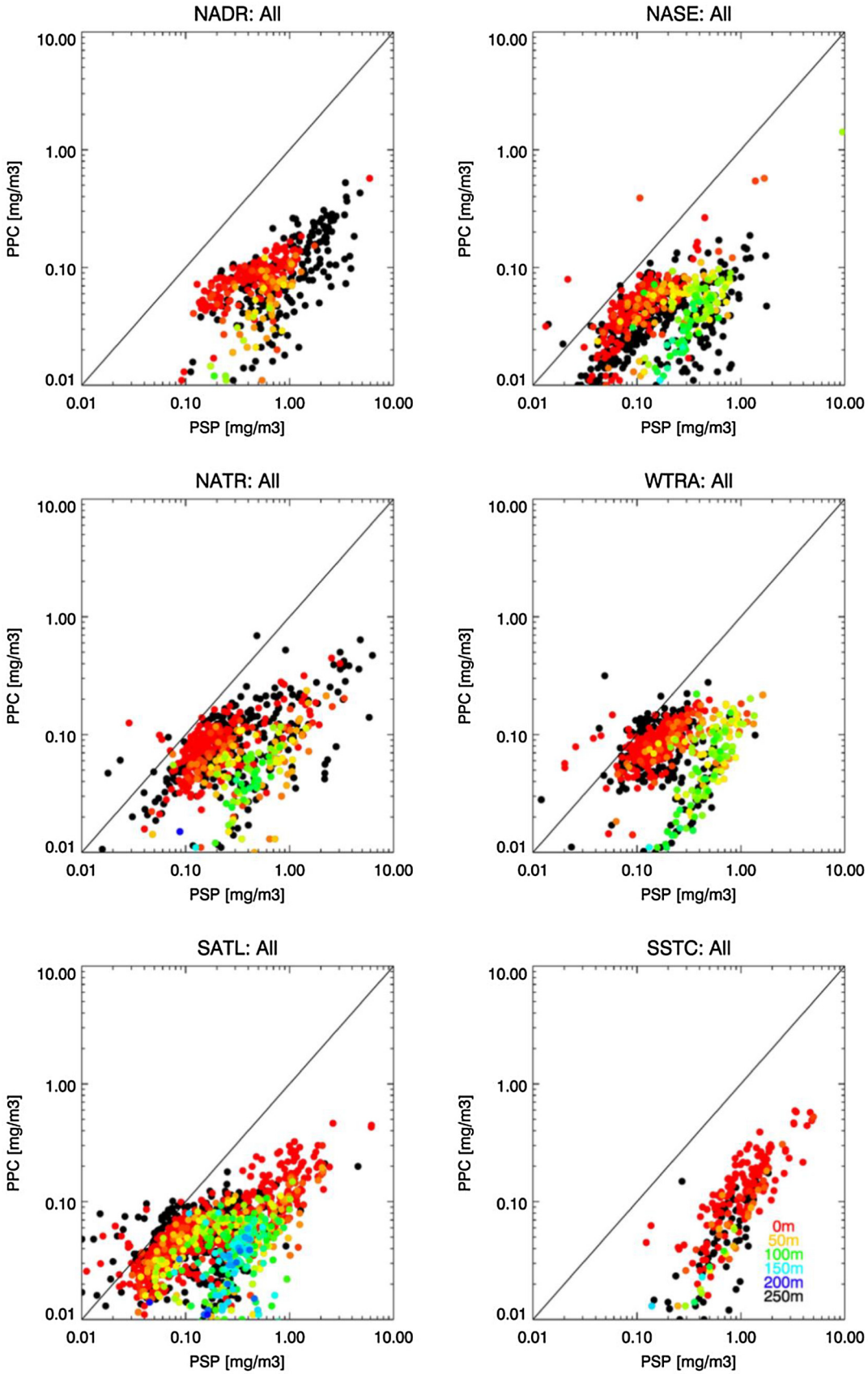

Fig. 12. Variation of Photoprotective Carotenoids (PPC) versus Photosynthetic Pigments (PSP) determined using HPLC analysis for six Longhurst provinces. The position that the samples were taken in the water column is colour coded. (For interpretation of the references to colour in this figure legend, the reader is referred to the web version of this article.)

Please cite this article in press as: Smyth, T., et al. Determining Atlantic Ocean province contrasts and variations. Prog. Oceanogr. (2017), http://dx.doi.org/10.1016/j.pocean.2016.12.004

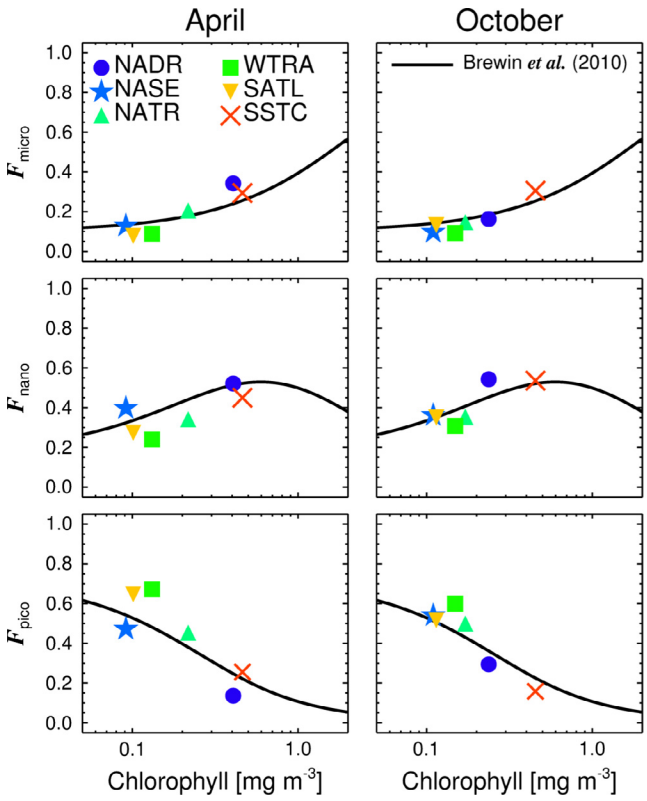

Fig. 13. Average fractions of pico- (cells <2 μm, denoted F_{pico}), nano- (cells 2–20 μm, denoted F_{nano}) and microphytoplankton (cells >20 μm, denoted F_{micro}) to total chlorophyll, plotted as a function of average total chlorophyll in each province.

data from the AMT transects shows that they can be present in waters as low as 8 °C, albeit at low abundances. In general they are better adapted to temperatures above 15 °C. Where temperatures are high enough, and nitrate >0.1 μM and there is sufficient light, then *Prochlorococcus* and *Synechococcus* seem to be able to coexist.

6.2.8. Phytoplankton pigments

The higher light levels in the sub-tropical and tropical provinces (NASE, NATR, WTRA and SATL) corresponded to a higher ratio of photoprotective carotenoids (PPC) to photosynthetic pigments (PSP) in surface waters (Fig. 12 – see also Aiken et al. (2009)). Indeed in some instances there is close to a 1:1 relationship of PPC:PSP. In these low latitudes, higher doses of UV radiation are experienced in the surface mixed layer (Smyth, 2011) than in the mid-latitude regions, this being a function of optical transparency, high surface irradiance and depth of the mixed layer. In the mid latitude provinces (NADR, SSTC) the ratio of PPC:PSP in surface waters was lower, driven by higher PSP. Notably in three of the four sub-tropical and tropical provinces (NASE, NATR and WTRA), the absolute amount of PPC forms a relatively tight cluster, particularly at the surface, and on moving to 50 or 100 m the main change is increase in PSP: there is less variation in PPC (Fig. 12). Notably, the chlorophyll component of PSP is tightly controlled according to light and nutrients to prevent phototoxicity. In addition, maintaining PPC could be a strategy of phytoplankton in sub-tropical and tropical provinces.

In addition to pigment composition, size structure also impacts many biogeochemical processes (Chisholm, 1992). Fig. 13 shows the average fractions of pico-, nano- and microphytoplankton in each province plotted as a function of total chlorophyll. Data follows relationships proposed by Brewin et al. (2010), with changes in size structure among provinces generally consistent with shifts in chlorophyll. Low latitude provinces (NASE, SATL, WTRA and NATR) are typically dominated by small phytoplankton (picoplankton), with the size of the phytoplankton shifting towards larger cells (nano- and microplankton) in higher latitude regions (SSTC and NADR).

The variation in pigment assemblage and composition may have implications for remote sensing algorithms in the different biomes (provinces) of the global ocean. Generally, algorithms to estimate chlorophyll concentration from ocean colour sensors such as SeaWiFS rely upon empirical band ratios. These relate reflectances at different optical wavelengths to the surface chlorophyll concentration (O' Reilly et al., 1998). Any subtle changes in the optical characteristics of the surface ocean, caused by variation in the pigment assemblage, may have a detrimental effect on estimates of chlorophyll using EO (IOCCG, 2014). This is likely to be particularly acute in the gyre regions where the lowest values of chlorophyll in the global ocean (<0.03 mg m^{-3}) are encountered. However, it is worth noting that such empirical band-ratio algorithms implicitly incorporate changes in the chlorophyll specific absorption coefficient, between low (gyre) and high (productive waters) chlorophyll concentrations, which in turn is characteristic of changes in pigment composition.

6.2.9. Optical Plankton Counter

The OPC has a limited range of particle sizes which it can detect, and in general the peak of the distribution for all the provinces is close to the lower limit of detection at between 247 and 322 μm (Table 2). This is to be expected as there are generally more small organisms than larger, consistent with the metabolic theory of ecology. Perhaps unsurprisingly the SATL has the lowest abundances of zooplankton (at the peak of the distribution) of all the

Table 2
Optical Plankton Counter (OPC) size distribution statistics for six Longhurst provinces. N "species" is the number of size bins that contain data within the province; N_{max} is the abundance of particles at the peak of the distribution. ESD is the Equivalent Sphere Diameter (μm) with ESD_{max} being the ESD at the distribution maximum and ESD_{med} that at the median peak of the distribution. σ_{peak} is the standard deviation at the peak of the distribution. All of these statistics are illustrated in Fig. 14 for the case of SATL.

Province	Season	N "species"	N_{max}	ESD_{max} (μm)	ESD_{med} (μm)	σ_{peak}	#Samples
NADR	*April*	609	694	287	247	27.92	17
	October	678	606	247	287	19.73	32
NASE	*April*	865	192	247	247	8.93	62
	October	765	103	247	247	5.08	61
NATR	*April*	1010	123	322	287	7.46	33
	October	869	411	287	247	17.77	60
WTRA	*April*	801	449	287	287	20.93	38
	October	867	1762	287	287	61.83	70
SATL	*April*	679	60	287	287	3.78	58
	October	1039	90	247	247	6.85	146
SSTC	*April*	635	104	247	287	4.20	10
	October	969	182	287	247	5.47	19

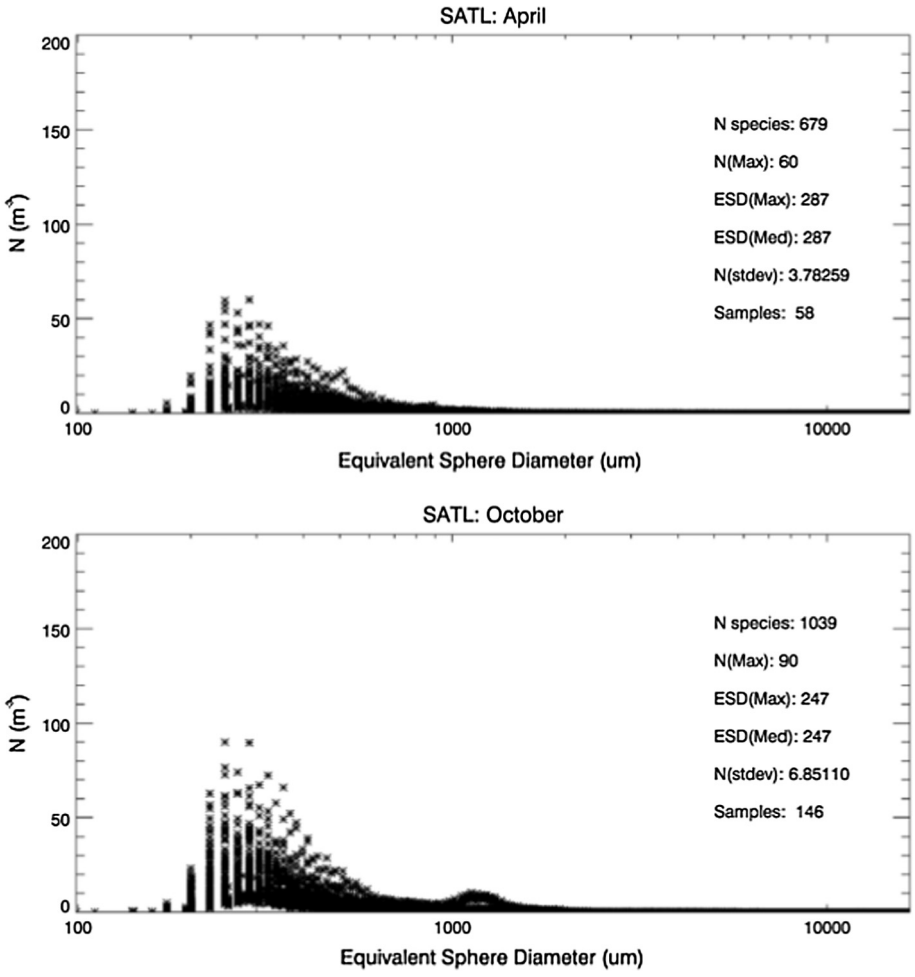

Fig. 14. Optical Plankton Counter (OPC) abundance (m^{-3}) versus size (μm) data for the SATL province.

provinces (Table 2 and Fig. 14) as this is where there is least resource (phytoplankton, nutrients). This shows only a limited amount of seasonality varying between 60 in April (autumn) and 90 in October (Spring) with a small amount of associated variation (±3.78 and ±6.85 respectively). However, it is the number of size bins which are populated with data, crudely assumed here to be representative of the number of species or a measure of biodiversity, which is somewhat surprising in the SATL. This ranges between 679 and 1039 in autumn and spring respectively.

A particular feature to note in Fig. 14 is the secondary peak in abundance around 1 mm ESD. Although this peak is an order of magnitude less than that of the primary peak, in terms of conversion to carbon biomass which is proportional to D^3, it will contain a larger percentage of the total. Most variation in the peak of the size distribution is shown in the productive NADR and the equatorial WTRA provinces, this is most likely due to the spatial (horizontal and vertical) heterogeneities in secondary production patterns.

As has already been alluded to, one of the disadvantages of using the OPC in isolation is that it only describes a small part of the total size spectrum (~0.25–16 mm). For a more complete description of the planktonic size distribution (covering six orders of magnitude in size) an array of different instrumentation and technologies are required such as flow cytometry, FlowCam and Plankton Visual Analyser (PVA) software in conjunction with preserved samples (San Martin et al., 2006). This has been done on a limited number of AMT transects allowing the investigation of metabolic scaling and trophic efficiency assumptions. These studies show the variation in the biomass spectra (bacteria to zooplankton) across the spread of the AMT provinces, in particular showing the change in spectral slope between the high and low latitudes. San Martin et al. (2006) observed a "dome-shaped" pattern in the slopes of community size spectra in the Atlantic, indicating a decrease in the trophic transfer efficiency of energy with increasing latitude and phytoplankton biomass.

7. Conclusions

The core *in situ* datasets presented in this paper, often considered as operationally necessary in support of hypothesis-driven science, have afforded observational insights into the contrasts between, and variations within, six major provinces of the Atlantic Ocean.

The different datasets used within this paper have elucidated different types of inter and intra-province contrasts and variation. Earth Observation (Primary Production, TKE) and modelling (NH Flux) has allowed spatial and temporal province contrasts and variation to be quantified. This covers the seasons and the months of the year which the *in situ* AMT sampling misses, as well as providing the wider spatial context.

The traits of the different provinces can be broadly categorised into two: the mid-latitude provinces (NADR and SSTC) and the subtropical, tropical and equatorial (NASE, NATR, WTRA and SATL). The mid-latitude provinces have strong seasonal signals which in turn drive greater amplitude in the spatial variation. This is particularly clear in the synoptic scale variation in the NH flux (Fig. 4a),

Please cite this article in press as: Smyth, T., et al. Determining Atlantic Ocean province contrasts and variations. Prog. Oceanogr. (2017), http://dx.doi.org/10.1016/j.pocean.2016.12.004

which is largely a result of changes in the SW flux, and in PP (Fig. 4c). The variation in these two parameters is progressively damped towards the equator with evidence for seasonal shifts apparent. Spatial variation in current driven TKE (Fig. 4c), although stronger in NADR and SSTC than three of the sub-tropical, tropical provinces (NASE, NATR and SATL), lacks the seasonal variation. The obvious outlier to this variation is in the equatorial WTRA province.

The *in situ* variation in temperature, salinity, oxygen and chlorophyll fluorescence also mirrors this broad categorisation. For *in situ* data it is possible to contrast the different provinces in terms of the amount of variation with depth and along the parts of the various transects within an individual province. The mid-latitudes are characterised by a seasonal stratification which in turn dictates the shape of the chlorophyll and oxygen profile. In general, these provinces exhibit a chlorophyll maximum within the surface mixed layer which corresponds to the maximum in oxygen, which shows little variation throughout the water column (20–50 μM). By contrast, the permanently stratified sub-tropical, tropical and equatorial regions have larger variation in the oxygen concentration (up to 200 μM) by virtue of poorer ventilation to the atmosphere. The sub-tropical and tropical provinces typically have a deep chlorophyll maxima (>70 m) which seasonally shoals and is offset from the oxygen maximum (by up to 87 m) as productivity is also a function of irradiance and nutrients as well as phytoplankton biomass.

Biologically the tropical and sub-tropical provinces show a tendency towards increased phytoplankton synthesis of photoprotective pigments in the surface layers. This has obvious energetic consequences for phytoplankton, making them less efficient in terms of primary productivity. This is directly related to increased incident solar irradiance in these regions and a deepening of the penetration depth of irradiance (i.e. clearer waters). Phytoplankton size structure shifted from smaller cells in low-latitude provinces towards larger cells in higher latitude regions.

Across the plankton spectrum, from small (cyanobacteria) to large (zooplankton) there are marked changes between the mid-latitude and sub-tropical/tropical provinces. The tropical provinces demonstrate strong relationships between *Prochlorococcus* and *Synechococcus* abundances throughout the water column which are not present in the mid-latitude provinces. At higher trophic levels, zooplankton becomes scarcer in the oligotrophic regions, but demonstrates greater diversity.

Acknowledgements

The authors thank the WHOI OAFlux project for providing the various heat flux model components. The altimeter products were produced by Ssalto/DUACS and distributed by Aviso with support from CNES. The primary production data were generated using the Ocean Colour Climate Change Initiative dataset, Version 1.0, European Space Agency, available online at http://www.esa-ocean-colour-cci.org. The authors would like to thank the crew of the various research vessels involved in AMT including RRS James Clark Ross, RRS Discovery and RRS James Cook; and the many originators of the datasets used. This study is a contribution to the international IMBER project and was supported by the UK Natural Environment Research Council National Capability funding to Plymouth Marine Laboratory and the National Oceanography Centre, Southampton. This is contribution number 306 of the AMT programme.

References

Aiken, J., Bale, A.J., 2000. An introduction to the Atlantic Meridional Transect (AMT) programme. Prog. Oceanogr. 45 (3–4), 251–256.

Aiken, J., Pradhan, Y., Barlow, R., Lavender, S., Poulton, A., Holligan, P., Hardman-Mountford, N., 2009. Phytoplankton pigments and functional types in the Atlantic Ocean: a decadal assessment, 1995–2005. Deep-Sea Res. Part II – Topical Stud. Oceanogr. 56 (15), 899–917. http://dx.doi.org/10.1016/j.dsr2.2008.09.017.

Arnault, S., Kestenare, E., 2004. Tropical Atlantic surface current variability from 10 years of TOPEX/Poseidon altimetry. Geophys. Res. Lett. 31 (3). http://dx.doi.org/10.1029/2003gl019210.

Barlow, R.G., Cummings, D.G., Gibb, S.W., 1997. Improved resolution of mono-and divinyl chlorophylls *a* and *b* and zeaxanthin and lutein in phytoplankton extracts using reverse phase C-8 HPLC. Mar. Ecol. Prog. Ser. 161, 303–307.

Blackford, J.C., Allen, J.I., Gilbert, F.J., 2004. Ecosystem dynamics at six contrasting sites: a generic modelling study. J. Mar. Sys. 52, 191–215.

Brewer, P.G., Riley, J.P., 1965. The automatic determination of nitrate in sea water. Deep Sea Res. 12, 765–772.

Brewin, R.J.W., Sathyendranath, S., Hirata, T., Lavender, S.J., Barciela, R.M., Hardman-Mountford, N.J., 2010. A three-component model of phytoplankton size class for the Atlantic Ocean. Ecol. Model. 221 (11), 1472–1483. http://dx.doi.org/10.1016/j.ecolmodel.2010.02.014.

Bryden, H.L., Longworth, H.R., Cunningham, S.A., 2005. Slowing of the Atlantic meridional overturning circulation at 25 degrees N. Nature 438 (7068), 655–657. http://dx.doi.org/10.1038/nature04385.

Brzezinski, M.A., 1985. The Si-C-N ratio of marine diatoms – interspecific variability and the effect of some environmental variables. J. Phycol. 21 (3), 347–357.

Campbell, J.W., 1995. The lognormal-distribution as a model for bio-optical variability in the sea. J. Geophys. Res. – Oceans 100 (C7), 13237–13254. http://dx.doi.org/10.1029/95jc00458.

Carr, M.E., Friedrichs, M.A.M., Schmeltz, M., Aita, M.N., Antoine, D., Arrigo, K.R., Asanuma, I., Aumont, O., Barber, R., Behrenfeld, M., Bidigare, R., Buitenhuis, E.T., Campbell, J., Ciotti, A., Dierssen, H., Dowell, M., Dunne, J., Esaias, W., Gentili, B., Gregg, W., Groom, S., Hoepffner, N., Ishizaka, J., Kameda, T., Le Quere, C., Lohrenz, S., Marra, J., Melin, F., Moore, K., Morel, A., Reddy, T.E., Ryan, J., Scardi, M., Smyth, T., Turpie, K., Tilstone, G., Waters, K., Yamanaka, Y., 2006. A comparison of global estimates of marine primary production from ocean color. Deep-Sea Res. Part II – Top. Stud. Oceanogr. 53 (5–7), 741–770. http://dx.doi.org/10.1016/j.dsr2.2006.01.028.

Chisholm, S.W., 1992. Phytoplankton size. In: Falkowski, P.G., Woodhead, A.D. (Eds.), Primary Productivity and Biogeochemical Cycles in the Sea, vol. 43, pp. 213–237.

de Mora, L., Butenschön, M., Allen, J.I., 2016. The assessment of a global marine ecosystem model on the basis of emergent properties and ecosystem function: a case study with ERSEM. Geoscientific Model Dev. 9, 59–76. http://dx.doi.org/10.5194/gmd-9-59-2016.

Deutsch, C., Sarmiento, J.L., Sigman, D.M., Gruber, N., Dunne, J.P., 2007. Spatial coupling of nitrogen inputs and losses in the ocean. Nature 445 (7124), 163–167. http://dx.doi.org/10.1038/nature05392.

Fairall, C.W., Bradley, E.F., Hare, J.F., Grachev, A.A., Edson, J.B., 2003. Bulk parameterization of air-sea fluxes: updates and verification for the COARE algorithm. J. Clim. 16 (4), 571–591.

Friedrichs, M.A.M., Carr, M.E., Barber, R.T., Scardi, M., Antoine, D., Armstrong, R.A., Asanuma, I., Behrenfeld, M.J., Buitenhuis, E.T., Chai, F., Christian, J.R., Ciotti, A.M., Doney, S.C., Dowell, M., Dunne, J., Gentili, B., Gregg, W., Hoepffner, N., Ishizaka, J., Kameda, T., Lima, I., Marra, J., Melin, F., Moore, J.K., Morel, A., O'Malley, R.T., O'Reilly, J., Saba, V.S., Schmeltz, M., Smyth, T.J., Tjiputra, J., Waters, K., Westberry, T.K., Winguth, A., 2009. Assessing the uncertainties of model estimates of primary productivity in the tropical Pacific Ocean. J. Mar. Syst. 76 (1–2), 113–133. http://dx.doi.org/10.1016/j.jmarsys.2008.05.010.

Fromentin, J.M., Powers, J.E., 2005. Atlantic bluefin tuna: population dynamics, ecology, fisheries and management. Fish Fish. 6 (4), 281–306. http://dx.doi.org/10.1111/j.1467-2979.2005.00197.x.

Garzoli, S.L., Garraffo, Z., 1989. Transports, frontal motions and eddies at the brazil-malvinas currents confluence. Deep-Sea Res. Part A – Oceanogr. Res. Papers 36 (5), 681–703. http://dx.doi.org/10.1016/0198-0149(89)90145-3.

Grasshoff, H., 1976. Methods of Sea Water Analysis. Verlag chemie, Weinheim.

Gruber, N., Sarmiento, J.L., 1997. Global patterns of marine nitrogen fixation and denitrification. Global Biogeochem. Cycles 11 (2), 235–266. http://dx.doi.org/10.1029/97gb00077.

Hardman-Mountford, N.J., Hirata, T., Richardson, K.A., Aiken, J., 2008. An objective methodology for the classification of ecological pattern into biomes and provinces for the pelagic ocean. Remote Sens. Environ. 112 (8), 3341–3352. http://dx.doi.org/10.1016/j.rse.2008.02.016.

Hemsley, V.S., Smyth, T.J., Martin, A.P., Frajka-Williams, E., Thompson, A.F., Damerell, G., Painter, S.C., 2015. Estimating oceanic primary production using vertical irradiance and chlorophyll profiles from ocean gliders in the North Atlantic. Environ. Sci. Technol. 49, 11612–11621. http://dx.doi.org/10.1021/acs.est.5b00608.

Herman, R.W., 1992. Design and calibration of a new optical plankton counter capable of sizing small zooplankton. Deep-Sea Res. 39, 395–415.

Hooker, S.B., Rees, N.W., Aiken, J., 2000. An objective methodology for identifying oceanic provinces. Prog. Oceanogr. 45 (3–4), 313–338. http://dx.doi.org/10.1016/s0079-6611(00)00006-9.

Hydes, D., Aoyama, M., Aminot, A., Bakker, K., Becker, S., Coverly, S., Daniel, A., Dickson, A.G., Grosso, O., Kerouel, R., van Ooijen, J., Sato, K., Tanhua, T., Woodward, E.M.S., Zhang, J.Z., 2010. Recommendations for the determination of nutrients in seawater to high levels of precision and inter-comparability using

continuous flow analysers. The GO-SHIP Repeat Hydrography Manual: A Collection of Expert Reports and Guidelines, vol. 134 (IOCCP Report).
IOCCG, 2014. Phytoplankton functional types from space. In: Sathyendranath, S. (Ed.), Technical Report. Reports of the International Ocean-Colour Coordinating Group, vol. 15. IOCCG, Dartmouth, Canada.
Jeffrey, S.W., Wright, S.W., 1997. Qualitative and quantitative HPLC analysis of SCOR reference algal cultures. In: Jeffrey, S.W., Mantoura, R.F.C., Wright, S.W. (Eds.), Phytoplankton Pigments in Oceanography: Guidelines to Modern Methods. UNESCO, Paris, p. 383.
Kamatani, A., 1982. Dissolution rates of silica from diatoms decomposing at various temperatures. Mar. Biol. 68 (1), 91–96. http://dx.doi.org/10.1007/bf00393146.
Karstensen, J., Stramma, L., Visbeck, M., 2008. Oxygen minimum zones in the eastern tropical Atlantic and Pacific oceans. Prog. Oceanogr. 77 (4), 331–350. http://dx.doi.org/10.1016/j.pocean.2007.05.009.
Kirkwood, D.S., 1989. Simultaneous Determination of Selected Nutrients in Sea Water, Vol. C.M. 1989/C:29: ICES Council Meeting Papers.
Le Traon, P.Y., Nadal, F., Ducet, N., 1998. An improved mapping method of multisatellite altimeter data. J. Ocean. Technol. 15, 522–534.
Le Traon, P.Y., Ogor, F., 1998. ERS-1/2 orbit improvement using TOPEX/POSEIDON: the 2cm challenge. J. Geophys. Res. – Oceans 103, 8045–8057.
Leterme, S.C., Pingree, R.D., 2008. The Gulf Stream, rings and North Atlantic eddy structures from remote sensing (Altimeter and SeaWiFS). J. Mar. Syst. 69 (3–4), 177–190. http://dx.doi.org/10.1016/j.jmarsys.2005.11.022.
Longhurst, A., 1998. Ecological Geography of the Sea. Academic Press, San Diego.
Longhurst, A., Sathyendranath, S., Platt, T., Caverhill, C., 1995. An estimate of global primary production in the ocean from satellite radiometer data. J. Plankton Res. 17 (6), 1245–1271. http://dx.doi.org/10.1093/plankt/17.6.1245.
Mann, D.G., 1999. The species concept in diatoms. Phycologia 38 (6), 437–495. http://dx.doi.org/10.2216/i0031-8884-38-6-437.1.
Montgomery, R.B., Wooster, W.S., 1954. Thermosteric anomaly and the analysis of serial oceanographic data. Deep-Sea Res. 2, 63–70.
Moore, C.M., Mills, M.M., Achterberg, E.P., Geider, R.J., LaRoche, J., Lucas, M.I., McDonagh, E.L., Pan, X., Poulton, A.J., Rijkenberg, M.J.A., Suggett, D.J., Ussher, S.J., Woodward, E.M.S., 2009. Large-scale distribution of Atlantic nitrogen fixation controlled by iron availability. Nat. Geosci. 2 (12), 867–871. http://dx.doi.org/10.1038/ngeo667.
Moore, C.M., Mills, M.M., Arrigo, K.R., Berman-Frank, I., Bopp, L., Boyd, P.W., Galbraith, E.D., Geider, R.J., Guieu, C., Jaccard, S.L., Jickells, T.D., La Roche, J., Lenton, T.M., Mahowald, N.M., Maranon, E., Marinov, I., Moore, J.K., Nakatsuka, T., Oschlies, A., Saito, M.A., Thingstad, T.F., Tsuda, A., Ulloa, O., 2013. Processes and patterns of oceanic nutrient limitation. Nat. Geosci. 6 (9), 701–710. http://dx.doi.org/10.1038/ngeo1765.
Morel, A., 1991. Light and marine photosynthesis: a spectral model with geochemical and climatological implications. Prog. Oceanog. 26, 263–306.
O'Reilly, J.E., Maritorena, S., Mitchell, B.G., Siegel, D.A., Carder, K.L., Garver, S.A., Kahru, M., McClain, C., 1998. Ocean color chlorophyll algorithms for SeaWiFS. J. Geophys. Res. 103, 24937–24953.
Palter, J.B., Sarmiento, J.L., Gnanadesikan, A., Simeon, J., Slater, R.D., 2010. Fueling export production: nutrient return pathways from the deep ocean and their dependence on the Meridional Overturning Circulation. Biogeosciences 7 (11), 3549–3568. http://dx.doi.org/10.5194/bg-7-3549-2010.
Partensky, F., Hess, W.R., Vaulot, D., 1999. Prochlorococcus, a marine photosynthetic prokaryote of global significance. Microbiol. Mol. Biol. Rev. 63 (1), 106.
Platt, T., Sathyendranath, S., 1988. Oceanic primary production - estimation by remote-sensing at local and regional scales. Science 241 (4873), 1613–1620. http://dx.doi.org/10.1126/science.241.4873.1613.
Platt, T., Sathyendranath, S., Longhurst, A., 1995. Remote-sensing of primary production in the ocean – promise and fulfillment. Philos. Trans. Royal Soc. London Series B – Biol. Sci. 348 (1324), 191–201. http://dx.doi.org/10.1098/rstb.1995.0061.
Redfield, A.C., 1958. The biological control of chemical factors in the environment. Am. Sci. 46, 205–221.
Reygondeau, G., Longhurst, A., Martinez, E., Beaugrand, G., Antoine, D., Maury, O., 2013. Dynamic biogeochemical provinces in the global ocean. Global Biogeochem. Cycles 27 (4), 1046–1058. http://dx.doi.org/10.1002/gbc.20089.
Robinson, C., Holligan, P., Jickells, T., 2006. The Atlantic transect programme – preface. Deep-Sea Res. Part II – Top. Stud. Oceanogr. 53 (14–16), 1483–1484. http://dx.doi.org/10.1016/j.dsr2.2006.06.002.
Robinson, C., Holligan, P., Jickells, T., Lavender, S., 2009. The Atlantic Meridional Transect Programme (1995–2012) Foreword. Deep-Sea Res. Part II – Top. Stud. Oceanogr. 56 (15), 895–898. http://dx.doi.org/10.1016/j.dsr2.2008.10.005.
Saba, V.S., Friedrichs, M.A.M., Antoine, D., Armstrong, R.A., Asanuma, I., Behrenfeld, M.J., Ciotti, A.M., Dowell, M., Hoepffner, N., Hyde, K.J.W., Ishizaka, J., Kameda, T., Marra, J., Melin, F., Morel, A., O'Reilly, J., Scardi, M., Smith, W.O., Smyth, T.J., Tang, S., Uitz, J., Waters, K., Westberry, T.K., 2011. An evaluation of ocean color model estimates of marine primary productivity in coastal and pelagic regions across the globe. Biogeosciences 8 (2), 489–503. http://dx.doi.org/10.5194/bg-8-489-2011.
Saba, V.S., Friedrichs, M.A.M., Carr, M.E., Antoine, D., Armstrong, R.A., Asanuma, I., Aumont, O., Bates, N.R., Behrenfeld, M.J., Bennington, V., Bopp, L., Bruggeman, J., Buitenhuis, E.T., Church, M.J., Ciotti, A.M., Doney, S.C., Dowell, M., Dunne, J., Dutkiewicz, S., Gregg, W., Hoepffner, N., Hyde, K.J.W., Ishizaka, J., Kameda, T., Karl, D.M., Lima, I., Lomas, M.W., Marra, J., McKinley, G.A., Melin, F., Moore, J.K., Morel, A., O'Reilly, J., Salihoglu, B., Scardi, M., Smyth, T.J., Tang, S.L., Tjiputra, J., Uitz, J., Vichi, M., Waters, K., Westberry, T.K., Yool, A., 2009. Challenges of modeling depth-integrated marine primary productivity over multiple decades: a case study at BATS and HOT. Global Biogeochem. Cycles 24. http://dx.doi.org/10.1029/2009gb003655.
San Martin, E., Harris, R.P., Irigoien, X., 2006. Latitudinal variation in plankton size spectra in the Atlantic Ocean. Deep Sea Res. Part II 53, 1560–1572.
Sarmiento, J.L., Gruber, N., Brzezinski, M.A., Dunne, J.P., 2004. High-latitude controls of thermocline nutrients and low latitude biological productivity. Nature 427 (6969), 56–60. http://dx.doi.org/10.1038/nature02127.
Sathyendranath, S., Longhurst, A., Caverhill, C.M., Platt, T., 1995. Regionally and seasonally differentiated primary production in the North Atlantic. Deep-Sea Res. Part I – Oceanogr. Res. Papers 42 (10), 1773–1802. http://dx.doi.org/10.1016/0967-0637(95)00059-f.
Schlosser, C., Klar, J.K., Wake, B.D., Snow, J.T., Honey, D.J., Woodward, E.M.S., Lohan, M.C., Achterberg, E.P., Moore, C.M., 2014. Seasonal ITCZ migration dynamically controls the location of the (sub)tropical Atlantic biogeochemical divide. Proc. Natl. Acad. Sci. USA 111 (4), 1438–1442. http://dx.doi.org/10.1073/pnas.1318670111.
Smyth, T., Tilstone, G., Groom, S., 2005. Integration of radiative transfer into satellite models of ocean primary production. J. Geophys. Res. – Oceans 110 (C10). http://dx.doi.org/10.1029/2004JC002784.
Smyth, T.J., 2011. Penetration of UV irradiance into the global ocean. J. Geophys. Res. – Oceans 116. http://dx.doi.org/10.1029/2011jc007183.
Steele, D.J., Tarran, G.A., Widdicombe, C.E., Woodward, E.M.S., Kimmance, S.A., Franklin, D.J., Airs, R.L., 2015. Abundance of a chlorophyll *a* precursor and the oxidation product hydroxychlorophyll a during seasonal phytoplankton community progression in the Western English Channel. Prog. Oceanogr. 137, 434–445. http://dx.doi.org/10.1016/j.pocean.2015.04.021.
Stramma, L., Johnson, G.C., Sprintall, J., Mohrholz, V., 2008. Expanding oxygen-minimum zones in the tropical oceans. Science 320 (5876), 655–658. http://dx.doi.org/10.1126/science.1153847.
Tarran, G.A., Heywood, J.L., Zubkov, M.V., 2006. Latitudinal changes in the standing stocks of eukaryotic nano- and picophytoplankton in the Atlantic Ocean. Deep-Sea Res. II 53, 1516–1529.
Tilstone, G., Smyth, T., Poulton, A., Hutson, R., 2009. Measured and remotely sensed estimates of primary production in the Atlantic Ocean from 1998 to 2005. Deep Sea Res. Part II 56 (15), 918–930.
Tyrrell, T., 1999. The relative influences of nitrogen and phosphorus on oceanic primary production. Nature 400 (6744), 525–531. http://dx.doi.org/10.1038/22941.
Uitz, J., Claustre, H., Morel, A., Hooker, S.B., 2006. Vertical distribution of phytoplankton communities in open ocean: an assessment based on surface chlorophyll. J. Geophys. Res. – Oceans 111 (C8). http://dx.doi.org/10.1029/2005jc003207.
Welschmeyer, N.A., 1994. Fluorometric analysis of chlorophyll-*a* in the presence of chlorophyll-*b* and pheopigments. Limnol. Oceanogr. 39 (8), 1985–1992.
Williams, P.J.L., Jenkinson, N.W., 1982. A transportable microprocessor-controlled precise Winkler titration suitable for field station and shipboard use. Limnol. Oceanogr. 27 (3), 576–584.
Winchester, S., 2011. Atlantic: A Vast Ocean of a Million Stories. HarperPress, UK.
Woodward, E.M.S., Rees, A.P., 2002. Nutrient distributions in an anticyclonic eddy in the North East Atlantic Ocean, with reference to nanomolar ammonium concentrations. Deep Sea Res. II 48, 775–794.
Yool, A., Tyrrell, T., 2003. Role of diatoms in regulating the ocean's silicon cycle. Global Biogeochem. Cycles 17 (4). http://dx.doi.org/10.1029/2002gb002018.
Yu, L., Jin, X., Weller, R.A., 2008. Multidecade Global Flux Datasets From the Objectively Analyzed Air-Sea Fluxes (OAFlux) Project: Latent and Sensible Heat Fluxes, Ocean Evaporation, and Related Surface Meteorological Variables. Woods Hole Oceanographic Institution, OAFlux Project Technical Report. OA-2008-01. Woods Hole Oceanographic Institution, Massachusetts, p. 64.
Zamora, L.M., Landolfi, A., Oschlies, A., Hansell, D.A., Dietze, H., Dentener, F., 2010. Atmospheric deposition of nutrients and excess N formation in the North Atlantic. Biogeosciences 7 (2), 777–793.
Zapata, M., Rodriguez, F., Garrido, J.L., 2000. Separation of chlorophylls and carotenoids from marine phytoplankton: a new HPLC method using a reversed phase C-8 column and pyridine-containing mobile phases. Mar. Ecol. Prog. Ser. 195, 29–45. http://dx.doi.org/10.3354/meps195029.
Zhang, J.Z., Chi, J., 2002. Automoted analysis of nanomolar concentrations of phosphate in natural waters with liquid waveguide. Environ. Sci. Technol. 36, 1048–1053.
Zubkov, M.V., Fuchs, B.M., Tarran, G.A., Burkill, P.H., Amann, R., 2003. High rate of uptake of organic nitrogen compounds by Prochlorococcus cyanobacteria as a key to their dominance in oligotrophic oceanic waters. Appl. Environ. Microbiol. 69 (2), 1299–1304. http://dx.doi.org/10.1128/aem.69.2.1299-1304.2003.

Please cite this article in press as: Smyth, T., et al. Determining Atlantic Ocean province contrasts and variations. Prog. Oceanogr. (2017), http://dx.doi.org/10.1016/j.pocean.2016.12.004